WILEY | Hindawi

Research Article

Study on the Genetic Differences in Reservoir Characteristics Based on the Bidirectional Provenance of the Yanchang Formation in the Jiyuan Area, Ordos Basin, China

Qiang Tong [ID], Zhaohui Xia, Jixin Huang, Junchang Wu, Yusheng Wang, Zheng Meng, and Chaoqian Zhang

Research Institute of Petroleum Exploration and Development, PetroChina, Beijing 100083, China

Correspondence should be addressed to Qiang Tong; nwutongqiang@126.com

Ordos Basin is a Mesozoic sedimentary basin that underwent long-term evolution on the North China Craton. Many scholars have confirmed that in the Late Triassic, the basin was surrounded by ancient continents, and there were multiple provenance supply directions. Combined with the nature of the basement of the basin and the characteristics of the present structure, it is believed that the Jiyuan area is located in the central and western parts of the basin, spanning two first-level structural units, the Tianhuan Depression and the Yishan Ramp. This special geographical location makes Jiyuan area affected by bidirectional provenance. Controlled by the northwest and northeast depositional systems in the basin, Jiyuan area has accepted complex sedimentation and diagenesis, forming a low-porosity ultralow-permeability reservoir. However, the understanding of bidirectional provenance has been neglected in many previous studies on reservoir characteristics in the Jiyuan area. Therefore, the differential evolution of sedimentation and diagenesis caused by bidirectional provenance will cause serious deviations in the original understanding of reservoir characteristics in the Jiyuan area, which will inevitably affect subsequent exploration and development research work. In this paper, the mineral composition, physical properties, diagenesis, and diagenetic evolution of the Jiyuan area are studied by combining a large number of tests such as core physical properties, casting thin sections, scanning electron microscopy, cathodoluminescence, and X-ray diffraction. Then, the origins of reservoir development in two areas dominated by bidirectional provenance are analyzed and compared. Furthermore, the diagenetic facies are characterized by a cluster analysis of logging data, and finally, the reasons for the differences in reservoir distribution and the genetic mechanism between the Yinshan provenance area (YPA) and Alxa provenance area (APA) are obtained. The results show that, first, due to the different provenance, compared with the YPA, the reservoir pore space in the APA is better developed and the physical properties are better. Second, the clay mineral content and diagenesis are more important causes of reservoir differentiation, and the reservoir pores in the YPA are more affected by kaolinite and chlorite filling than those in the APA. Although more dissolution improvements have been obtained, the damage to the reservoir caused by cementation in the middle and late stages is extremely fatal, while the chlorite film in the APA reservoir has a better protection effect on the primary intergranular pores. Third, after the evolution of pores in the APA reservoir, more intergranular pores are preserved, and the distribution range of high-quality diagenetic facies is wider than that in the YPA. Finally, sedimentation is the basis for high-quality reservoir development, and good mineral content composition and favorable diagenetic transformation cause reservoir dissimilarity.

1. Introduction

The Ordos Basin has great potential for unconventional oil and gas resources, but it still faces many major challenges [1]. In recent years, as research on the lower assemblage of the Yanchang Formation has increased, predecessors have carried out a series of studies on the Chang 8 oil-bearing formation of the Yanchang Formation. In particular, the Chang 8_1 formation is the main formation. The macroscopic research aspects include sequence stratigraphic analysis [2],

sedimentary characteristics research [3], sandbody structure genesis research [4, 5], and fault zone development and distribution characteristics research [6]. The microscopic research aspects include the influence of diagenesis and densification upon accumulation [7–10], quantitative evaluation of the microscopic pore structure origin [11–13], and research on the characteristics of movable fluid and water flooding [14, 15]. The Jiyuan Oilfield is an important object of research within the Mesozoic Triassic reservoirs in the Ordos Basin [16–19]. After more than ten years of exploration and development, it has achieved a very large scale of production. However, the Jiyuan Oilfield has bidirectional provenances from the northwest and northeast [3, 20–23], so reservoir development is affected by mixed depositional sources [18, 22, 24–26]. In previous studies, the Jiyuan Oilfield has often been regarded as a whole [27], and the differences in reservoir characteristics between the Yinshan provenance area (YPA) and Alxa provenance area (APA) have been ignored, so the dissimilarity between reservoirs from those two directions during the depositional period of the Yanchang Formation in the Jiyuan Oilfield has not received obvious attention thus far [28–30]. An overview of the literature reveals that in terms of sedimentary environmental characteristics, main controlling factors, formation water distribution characteristics, and differences in oil reservoirs, predecessors have noticed the zoning between the differences in the geological characteristics in the Jiyuan area. However, most studies have not clearly proposed those differences, and the reasons for the differences have not been summarized. Therefore, this paper takes the Chang 8_2 reservoir in the Jiyuan Oilfield, which has received relatively little attention from predecessors, as the research object; as exploration deepens, it will receive more attention. More importantly, this paper conducts a comparative study on the origin of reservoir characteristics in the YPA and APA of the Jiyuan Oilfield based on a comparison of reservoir petrology and physical property differences. The types of diagenesis and diagenetic evolution characteristics are studied in combination with core physical properties, casting thin sections, scanning electron microscopy, cathodoluminescence, X-ray diffraction, and other analytical and test results. Based on diagenetic facies division, cluster analysis is used to complete a diagenetic facies logging discrimination, and the differences in reservoir development between the YPA and APA are clarified by the plane distribution of diagenetic facies. In addition, the differences in the formation mechanism of the reservoirs in the YPA and APA are elucidated via three aspects: sedimentation, mineral content, and diagenetic transformation. Finally, a differential genetic model of the YPA and APA reservoirs is constructed, combined with the evolution differences of microscopic matrix pores, and the physical property comparison results caused by clay minerals and diagenesis are clarified. The purpose of this study is to provide guidance for the subsequent exploration and development of the target reservoirs in the Jiyuan Oilfield and to provide a theoretical basis for expanding the research on the differences in reservoir formation between the YPA and APA in the Jiyuan area.

2. Geological Setting

The Jiyuan Oilfield is located in the midwestern Ordos Basin, and its structure spans the Yishan Ramp and Tianhuan Depression [31–33] (Figure 1(a) and 1(b)). The structure in this area is gentle, and the stratum dip angle is small. The basement subsidence is stable, and the faults are not well developed. There are only locally developed low-amplitude basal eminences [21, 34]. The Ordos Basin was a large inland freshwater lake basin in the Late Triassic, and the Triassic Yanchang Formation is the main oil-producing reservoir (Figure 1(c)). This set of strata is divided into 10 oil-bearing formations from bottom to top, of which the Chang 8 sedimentary period is from the formation to the development of the lake basin, and the Chang 7 sedimentary period extends into the peak period of the lake basin [35]. The Chang 8 oil-bearing group is divided into the Chang 8_2 and Chang 8_1 sub-oil-bearing groups from bottom to top, with overall thicknesses of 75-90 m, of which the average thickness of the Chang 8_2 sub-oil-bearing group is approximately 40 m [2]. Because the topography of the lake basin was gentle and open and the slope was less than 0.5°, a shallow-water delta depositional system with underwater distributary channels as the main body was developed [3]. The location of the study area in this paper mainly includes Mahuangshan, Fengdikeng, Jiyuan, and Wangpanshan. Based on the combination of oilfield production practices and geological significance, we divided the reservoirs in the study area according to the northeast and northwest provenance directions. To simplify the text, the area that mainly provided by the Yinshan ancient land in the northeast is abbreviated YPA in this paper, and the area that mainly provided by the Alxa ancient land in the northwest is abbreviated APA in this paper. Therefore, the study area in the Jiyuan Oilfield is divided into the YPA and APA, and the number of controlled wells includes 540 in the frame (Figure 1(d).

3. Materials and Methods

3.1. Core Physical Property Analysis. This study focuses on the Upper Triassic Yangchang Formation sandstones in the midwestern Ordos Basin, where most of the producing oil fields are located, and consequently, where most drillings have occurred. More than 2357 reservoir porosity and permeability data points of Chang 8_2 were collected from the Research Institute of Petroleum Exploration and Development, Changqing Oilfield Company, PetroChina.

3.2. Geophysical Logging Analysis. Depending on the satisfactory response characteristics in the logging curves (i.e., types of association, amplitude, and abrupt/gradational top and base of gamma ray log (GR), acoustic log (AC), spontaneous potential log (SP), and shale content (SH)), the targeted stratum was identified. Then, by calibrating the depth of logging curves with the vertical position of the sample in the core, the diagenetic horizon represented by the photos that is consistent with the microscopic observations corresponds to the logging curve.
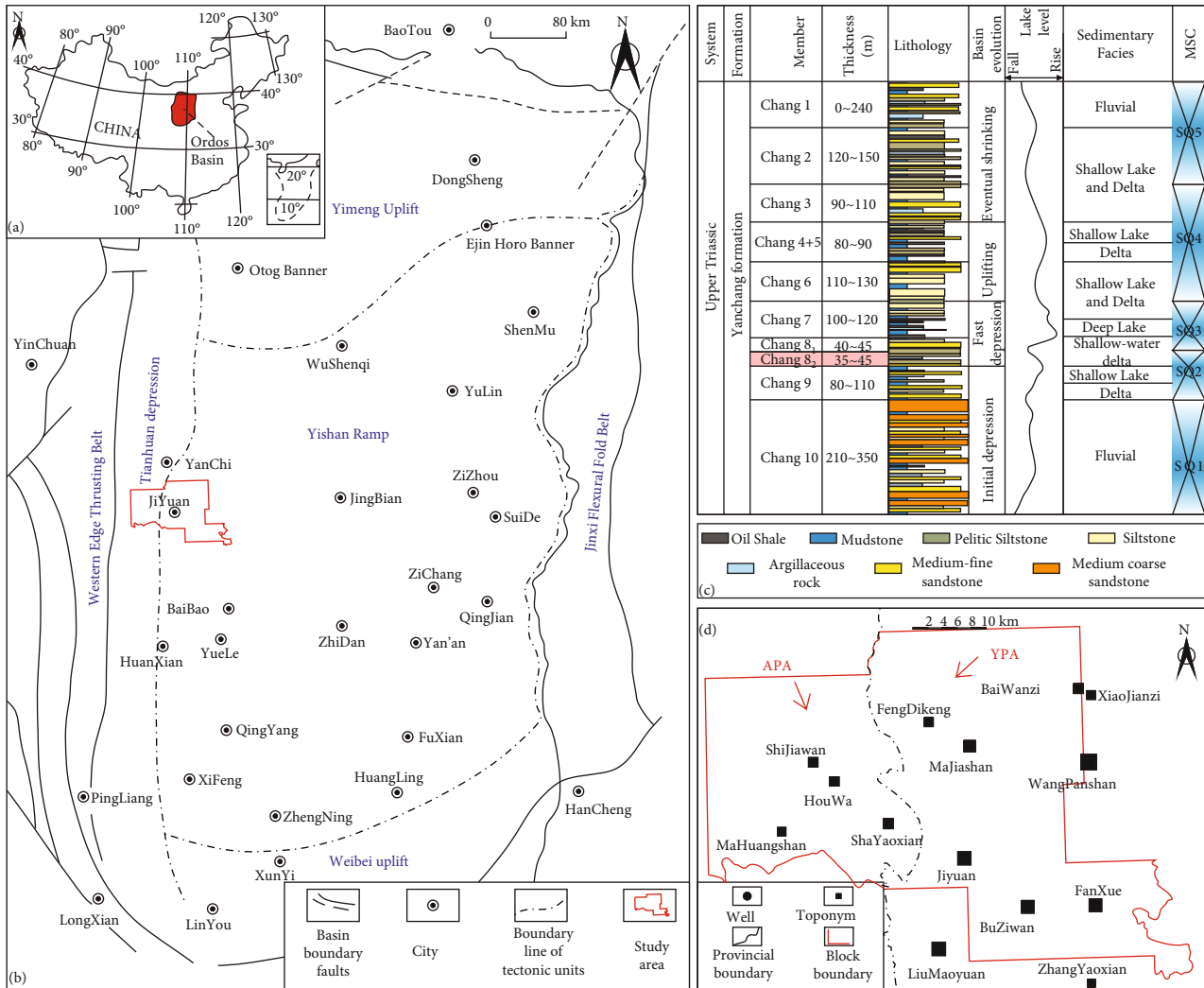
FIGURE 1: (a) Simplified map of China showing tectonic provinces and the location of the Ordos Basin; (b) map showing the tectonic subdivisions of the Ordos Basin and the location of the study area (modified after [31]); (c) stratigraphic table of the Ordos Basin showing Upper Triassic strata, the thickness of the 10 oil-bearing members of the Yanchang Formation and the associated lithology, basin evolution, sedimentary facies, and lake level fluctuations (modified after [33]); (d) specific location of the study area and the provenance direction that divides this area into the YPA and APA.

3.3. Casting Thin Sections, Scanning Electron Microscopy and Cathodoluminescence.

To accurately identify pore types and quantify porosity, casting thin sections were impregnated with red resin prior to sectioning. Part of each thin section was stained with alizarin red and potassium ferricyanide to distinguish carbonate minerals, with calcite showing as dark red and ferroan calcite showing as dark red to purple. Point counting was undertaken to obtain mineralogical compositions and authigenic mineral contents, with at least 400 point counts per thin section. The Udden–Wentworth grain size scale was used to determine the sandstone grain size [36, 37]. The large amount of casting thin section data were mainly provided by the Changqing Oilfield. Experts gathered the data under the microscope, and the data include the contents of various types of minerals, the types and contents of interstitial matter, the types and quantities of porosity space, the pore structure, and the plane porosity. Finally, the conclusions

attained from the microscope analysis, as well as the name of the rock, were obtained.

Based on petrographic analysis, major types of authigenic minerals and distinct pore spaces were analyzed using scanning electron microscopy (SEM) equipped with energy dispersive spectrometry. Samples were gold-coated and observed under a Quanta FEG 450 at an accelerating voltage of 20 keV to identify the pore geometry and cement morphology for the semiquantitative estimation of mineral compositions and documentation of the textural relationships between the minerals.

Cathodoluminescence (CL) imaging was used to identify the stage of carbonate cement using a Cambridge CL8200 MK5 detector (accelerating voltage of 13 kV; beam current of 250 μA) and a Leica optical microscope.

3.4. X-Ray Diffraction.

A total of 40 reservoir sandstone samples were analyzed for whole-rock (bulk) and clay

fraction (<2 μm) mineralogy using X-ray diffraction. The sample preparation, analysis, and interpretation procedures used by Moore and Reynolds [38] and Hillier [39] were adopted. Approximately 5.0 grams of each sample was crushed, milled in ethanol in a McCrone micronizing mill and then dried at 60 °C. Randomly oriented powders were prepared by top loading into polymethylmethacrylate (PMMA) sample holders designed with concentric circular geometry grooved shallow wells. The powder diffraction patterns were then collected using a D/MAX 2500 X-ray diffractometer with Cu Kα radiation. All X-ray diffraction (XRD) data were first analyzed for phase identification using the search–match module of evaluation (EVA) software and the reference databases of the International Center for Diffraction Data Powder Diffraction File 2 and Crystallography Open Database. After the phases were identified with EVA, they were further analyzed based on the Rietveld quantitative X-ray diffraction refinement approach.

3.5. Reservoir Densification Calculation Method. The pore evolution of sandstone is usually composed of two aspects. The primary pores are reduced by compaction, pressure, dissolution, and cementation, and the secondary pores are increased by dissolution. In this paper, the densification process of the reservoir is quantitatively characterized by indicators such as the visual compaction rate (VCOR), visual cementation rate (VCER), visual dissolution rate (VDR), and diagenetic coefficient (DC) [2, 11].

The visual compaction rate represents the degree of compaction of the original sediment pore space, which is calculated as follows. OPV is the original pore volume. IV is the interstitial volume. IPV is the intergranular pore volume.

$$VCR = \frac{OPV - IV - IPV}{OPV} \times 100\%. \qquad (1)$$

The original pore volume is calculated by the sorting coefficient S_p proposed by P.D. Trask:

$$OPV = 20.91 + \frac{22.9}{S_p}. \qquad (2)$$

The Trask sorting coefficient (S_p) is calculated from the particle size distribution of the debris sediment, where P_{25} is the particle size value at 25%, and P_{75} is the particle size value at 75%.

$$S_p = \sqrt{P_{25}/P_{75}}. \qquad (3)$$

The visual cementation rate indicates the degree of cementation of the reservoir reformation and is calculated as follows. CV is the cement volume.

$$VCER = \frac{CV}{OPV} \times 100\%. \qquad (4)$$

The visual dissolution rate represents the strength of dissolution and is calculated as follows. SDP is the secondary dissolution plane porosity. TP is the total plane porosity.

$$VDR = \frac{SDP}{TP} \times 100\%. \qquad (5)$$

The diagenesis coefficient indicates the comprehensive influence of diagenesis on the reservoir performance and is calculated as follows. MP is the microporosity. P represents the plane porosity.

$$DC = \frac{P}{VCR + VCER + MP}. \qquad (6)$$

The microporosity is calculated by the following formula. MPO is the measured physical porosity.

$$MP = \frac{MPO - P}{MPO} \times 100\%. \qquad (7)$$

The calculation results of the above parameters quantitatively characterize the reservoir densification process.

3.6. Lithoelectric Calibration and Diagenetic Facies Division Method. Since the mineral content and physical property parameters of different types of diagenetic facies have certain rules, the diagenetic facies corresponding to high-quality reservoirs have better pore throat structure, pore, and permeability characteristics, so the three types of porosity log curves play a role in identification. With the addition of oil-bearing properties, the resistivity (RT) curve also changes, and the lithology can be assessed by using curves such as SP, GR, and PE. In this paper, the core location is completed by the mutual calibration of the porosity of the core and the AC logging curve [2, 40, 41].

The diagenetic facies division in this paper is mainly based on the analytical results of the casting thin sections. This paper focuses on the classification of diagenetic facies types according to the clay mineral contents and pore space characteristics in the mineral components [42]. The advantage of this division method is that it can indicate the petrophysical properties of the diagenetic facies in the log curve parameter changes, which is helpful for the effective completion of the lithoelectric calibration [43].

3.7. Cluster Analysis Method. The cluster analysis was mainly carried out by SPSS software (Statistical Product Service Solutions of IBM Corporation). First, the collinearity diagnosis of different logging curves was carried out, and the non-independent logging curve parameter types were eliminated. The type of logging curve that remains indicates that the parameters do not have multicollinearity. Then, discriminant analysis was carried out to obtain the group statistical results. Finally, the Fisher discriminant function was used to establish the discriminant relationship of different diagenetic facies types, and the group centroid distribution map that is automatically produced by the software was obtained.
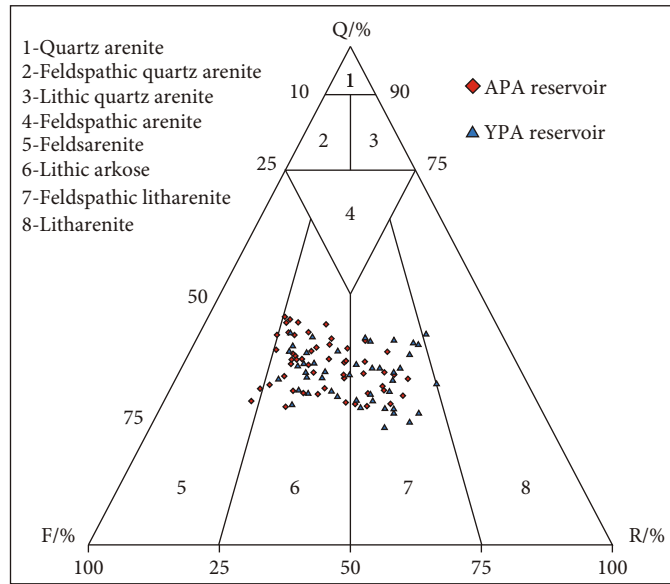
(a)
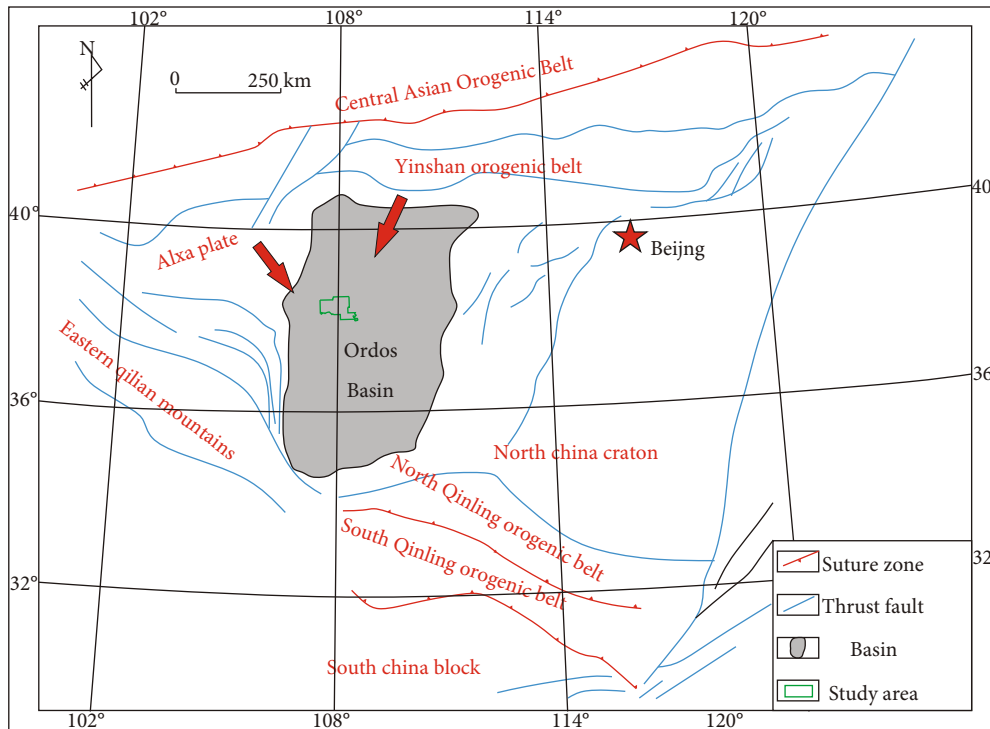
(b)

FIGURE 2: (a) Classification of sandstone in the Chang 8_2 reservoir in the YPA and APA using the Chinese industry standard [44]; (b) bidirectional Provenance Location modified from [24].

4. Results and Interpretations

4.1. Reservoir Petrological Characteristics

4.1.1. Rock Classification and Clastic Assemblage. According to the statistics of 57 casting thin section samples from the Chang 8_2 reservoir in the APA and 46 samples from the Chang 8_2 reservoir in the YPA in the study area, the rock types are mainly lithic arkose and feldspathic litharenite

(Figure 2). Among them, the average quartz content in the APA is 34.38%, the average feldspar content is 37.55%, and the average rock fragment content is 28.07%. The average quartz content in the YPA is 36.8%, the average feldspar content is 32.43%, and the average rock fragment content is 30.72%, indicating that the compositional maturity in the YPA is slightly higher than that in the APA, which is related to the farther provenance in the YPA (Table 1). For the rock fragment contents, metamorphic rock fragments

TABLE 1: Differential statistics of the clastic component contents between the Chang 8_2 reservoir in the YPA and APA in the Jiyuan area.

Distribution	Quartz %	Feldspar %	Rock fragment %	Igneous %	Metamorphic %	Sedimentary %
APA	28.45	31.65	23.37	9.07	14.03	0.27
YPA	31.49	27.93	25.87	10.07	14.96	0.84
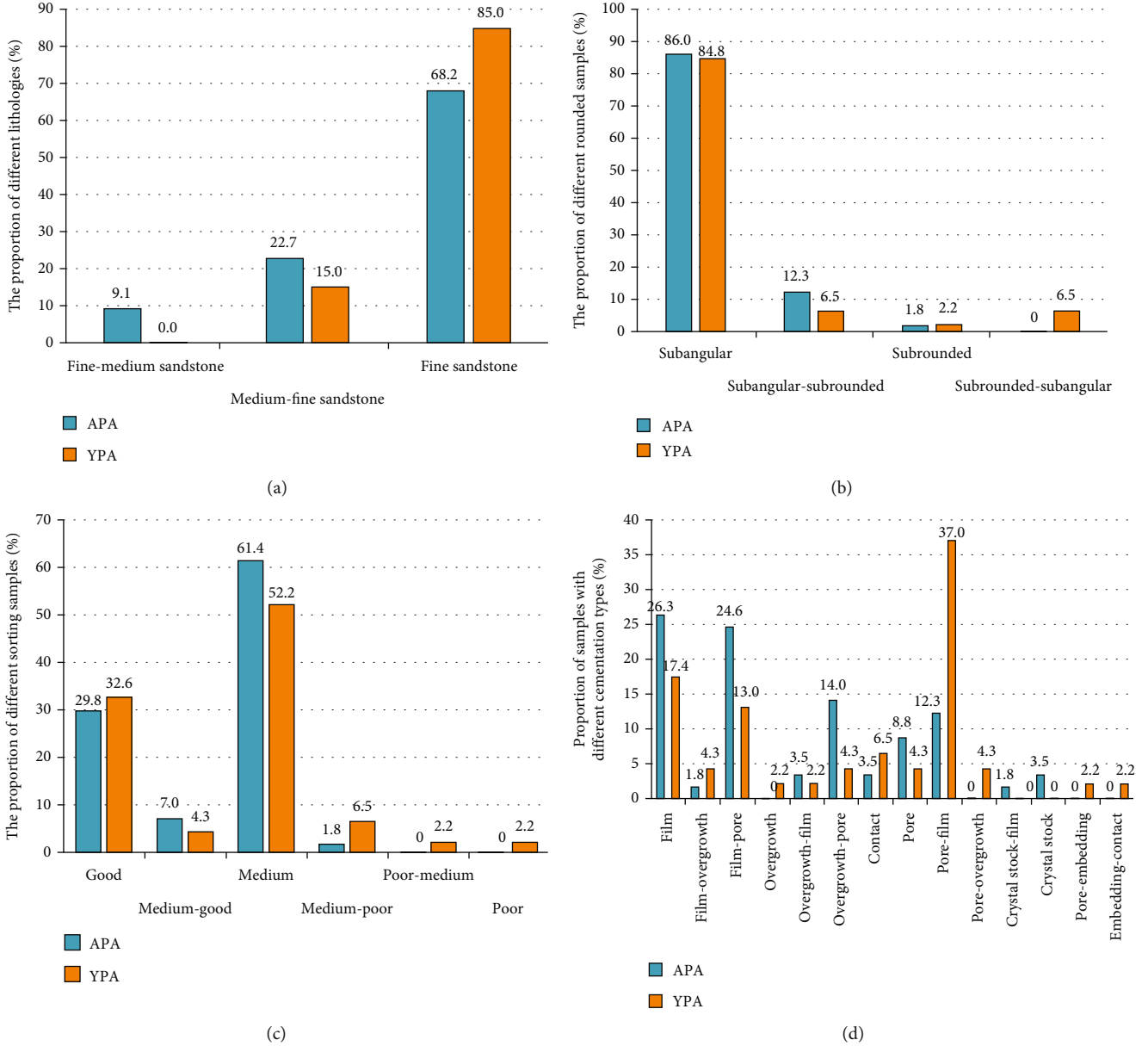
FIGURE 3: Comparison of rock differences between the Chang 8_2 reservoirs in the APA and YPA. (a) Comparison of lithologic differences between the YPA and APA. (b) Comparison of rounding differences between the YPA and APA reservoirs. (c) Comparison of reservoir sorting differences between the YPA and APA. (d) Comparison of cementation types between the YPA and APA.

have the highest contents in the YPA and APA, followed by igneous rock fragment contents, but the content of the three types of rock fragments in the APA is slightly lower than that in the YPA.

4.1.2. Reservoir Rock Characteristics.
The reservoir rock structure data from 103 thin sections were counted, and

image grain size analysis was carried out in combination with 20 samples from the YPA reservoir and 22 samples from the APA reservoir (Figure 3).

The grain size of the Chang 8_2 reservoir is mainly fine to medium, and the number of samples with this grain size in the APA is greater than that in the YPA (Figure 3(a). The rounding in the APA is slightly less than that in the YPA,
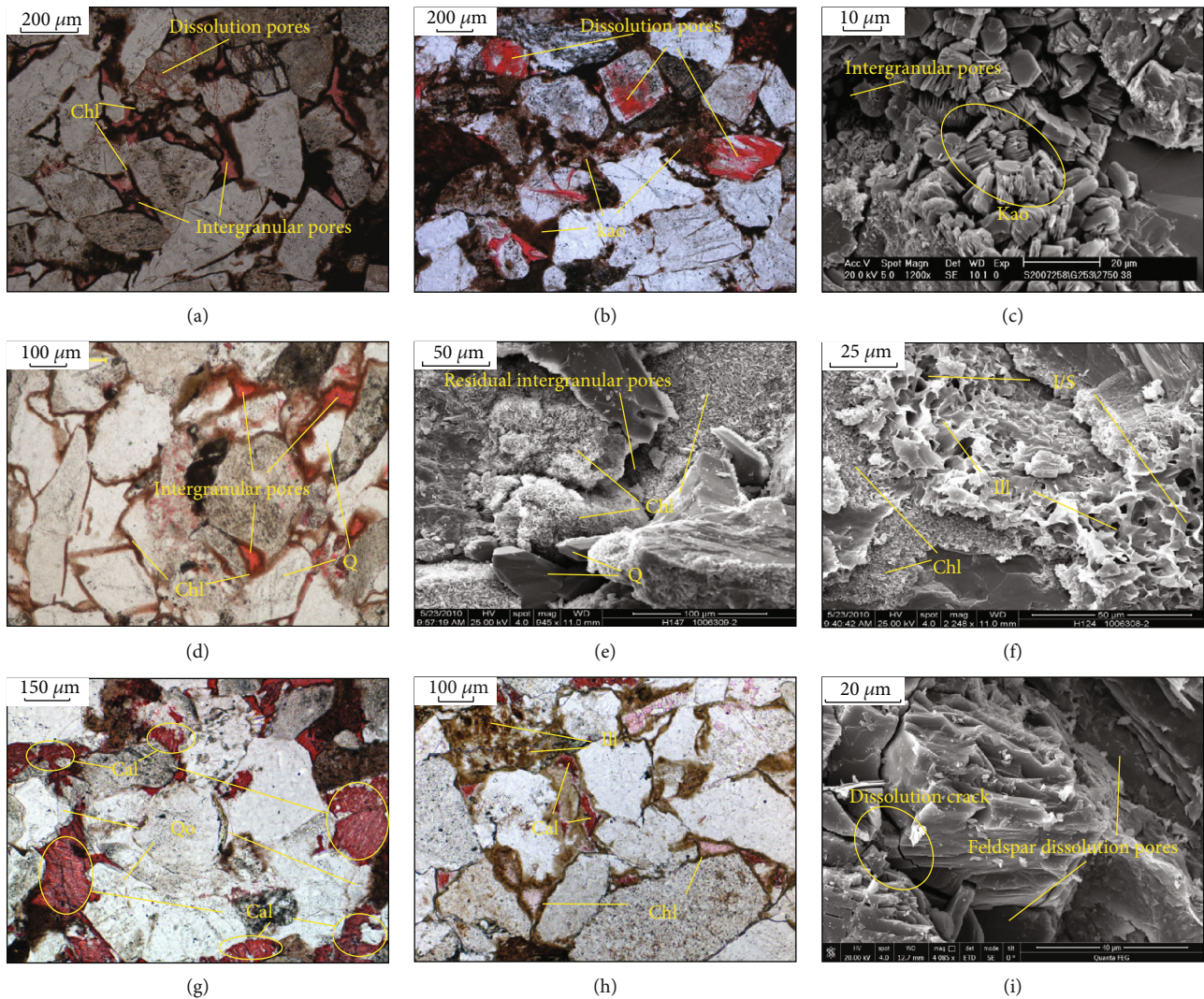
FIGURE 4: Pore types and filling mineral compositional characteristics of the Chang 8_2 reservoir in the study area. (a) YPA, chlorite film filling pores. Chl stands for chlorite. (b) YPA, kaolinite fills the pores, and dissolved pores are visible. Kao stands for kaolinite. (c) APA, book-like kaolinite filling intergranular pores. (d) YPA, chlorite film, and intergranular pores and siliceous filling pores. Q stands for quartz. (e) APA, quartz overgrowths, and chlorite and authigenic quartz are distributed on the grain surface and in the intergranular pores. (f) YPA, illite, and I/S mixed layers are distributed in the dissolution pores, and chlorite is distributed on the grain surface. Ill stands for illite, and I/S stands for illite/smectite mixed layer. (g) APA, quartz overgrowths are common, and calcite fills the pores and metasomatizes debris. Qo stands for quartz overgrowth. (h) YPA, chlorite film is developed, and calcite and authigenic illite fill the pores. Cal stands for calcite. (i) APA, feldspar dissolution produces dissolution pores and intragranular cracks.

and the subangular samples account for a larger proportion (Figure 3(b). The sorting in the APA is less than that in the YPA, and the proportion of well-sorted samples is lower than that in the YPA (Figure 3(c). There are great differences in the types of cementations between the YPA and APA. The APA is dominated by film cementation and film–pore cementation, but the YPA is dominated by pore–film cementation (Figure 3(d).

4.1.3. Interstitial Composition and Characteristics. Microscopic observations revealed that the interstitials in the study area are rich in clay minerals, carbonate cement, and siliceous content (Figure 4). The chlorite on the particle surface protects the remaining intergranular pores and fills locally (Figure 4(a). Kaolinite fills the intergranular pores and local

dissolution pores (Figures 4(b) and 4(c). Silica-filled pores and authigenic quartz-filled residual intergranular pores protected by chlorite film are also common [45] (Figures 4(d) and 4(f). Dissolution pores filled by illite and I/S mixed layers are also common (Figure 4(f). Calcite fills the pores, reducing the plane porosity (Figures 4(g) and 4(h). The pores and dissolution cracks produced by dissolution are also visible, but they have not been filled locally, indicating that dissolution in the study area has a great influence on the pore space of the reservoir (Figure 4(i).

According to the CTS results, the interstitial statistics show that the average interstitial content in the APA is higher than that in the YPA (Table 2).

The contents of chlorite and kaolinite in the APA are lower than those in the YPA, while the contents of illite

TABLE 2: Statistics of the interstitial content in the Chang 8_2 reservoir in the Jiyuan area.

Distribution	Total interstitial material (%)	Clay minerals (%)				Carbonate cement (%)			Siliceous (%)	Other (%)					
		Kao	Ill	Chl	Cal	Ferro-calcite	Dolomite	Ankerite		Feld-spar	Siderite	Tuffaceous	Barite	Pyrite	Laumontite
APA	11.69	0.48	1.54	4.70	1.64	4.32	0.00	0.24	1.61	0.22	0.00	0.04	0.05	0.13	0.56
YPA	10.61	0.90	1.29	5.05	0.69	2.58	0.00	0.00	1.85	0.17	0.00	0.00	0.03	0.25	0.03

TABLE 3: Statistical results of XRD in the YPA and APA.

Distribution	Value	Ill %	I/S %	Kao %	Chl %	Ill in I/S %	Porosity %	Permeability mD
APA (n: 20)	Maximum	45.29	16.08	28.48	97.25	90	18.28	21.58
	Minimum	1.25	0.00	0.00	22.48	70	2.17	0.013
	Average	21.72	8.25	7.06	62.97	80	9.96	2.97
YPA (n: 20)	Maximum	37.59	21.25	43.25	91.93	95	15.03	6.59
	Minimum	5.32	0.65	0.00	24.24	80	2.06	0.004
	Average	14.43	5.48	8.36	71.74	90	6.40	1.29
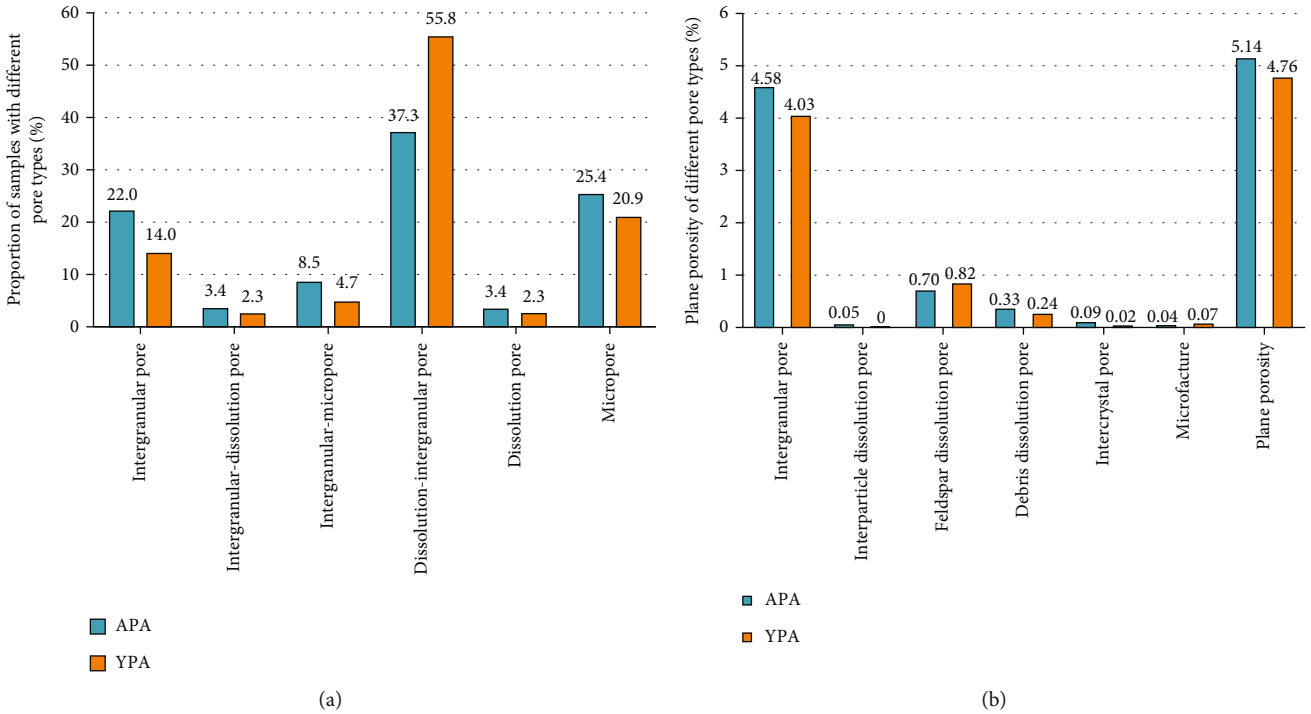
FIGURE 5: Comparison of reservoir space types and characteristics between the YPA and APA. (a) Proportion of samples with different pore types in the YPA and APA reservoirs. (b) Plane porosity differences of six pore types in the YPA and APA.

are higher than those in the YPA. Among the differences in carbonate cement, the contents of calcite and ferrocalcite in the APA are higher than those in the YPA. In addition, the siliceous content in the APA is lower than that in the YPA.

Among other interstitial materials, the feldspathic content in the APA is slightly higher than that in the YPA, and the laumontite content is significantly higher than that in the YPA; however, the content of pyrite is slightly lower than that in the YPA. Among them, more carbonate cements are represented by chlorite, clay minerals, ferrocalcite, and calcite, and the silica content is higher.

In the study area, clay minerals account for a large proportion of interstitials and have a significant impact on reservoir physical properties [46]. The clay mineral content was quantified by XRD experiments, and the results are as follows (Table 3).

X-ray diffraction data are consistent with the overall distribution trend of the contents of different types of clay minerals in thin sections. The contents of illite and I/S mixed layers in the APA are higher than those in the YPA, while the kaolinite content in the APA is lower than that in the YPA. The chlorite content in the APA is lower than that in the YPA. Therefore, except for the chlorite film that forms a large number of pore liners, the chlorite pore filling degree in the YPA is higher.

4.1.4. Types and Characteristics of Reservoir Pore Space. The reservoir spaces in the YPA and APA of the Chang 8_2 reservoir in the study area are dominated by dissolved pores and intergranular pores, followed by micropores and intergranular pores (Figure 5).

The proportion of dissolved pores and intergranular pores in the APA reservoir is lower than that in the YPA reservoir, while the proportion of intergranular pores in the APA reservoir is higher than that in the YPA reservoir. In addition, the proportion of micropores in the APA is higher than that in the YPA, indicating that the proportion of small pores in the APA is greater, and the impact on the reservoir remains to be explored (Figure 5(a)).

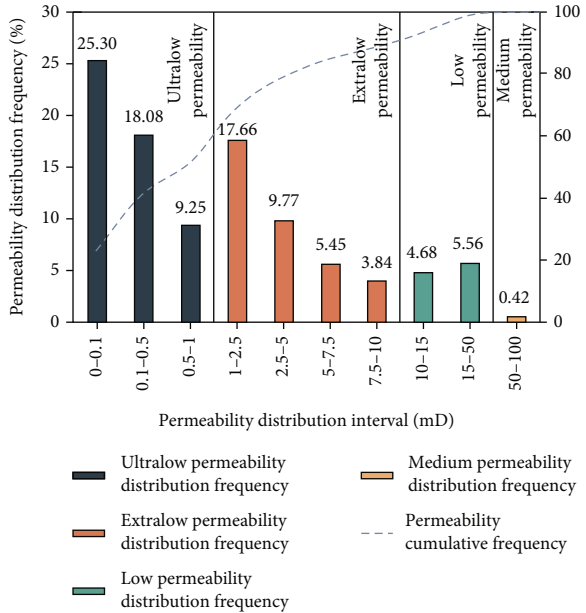TABLE 4: Physical property parameters of the core analysis (according to [47]).

Distribution	Number of samples	Porosity/%		Horizontal permeability/$10^{-3}\mu m^2$	
		Range	Average	Range	Average
Overall	2357	0.92-18.89	11.88	0.002-64.267	2.997
APA	1925	0.92-18.89	12.14	0.002-64.267	3.573
YPA	432	2.53-16.18	10.71	0.002-5.578	0.431
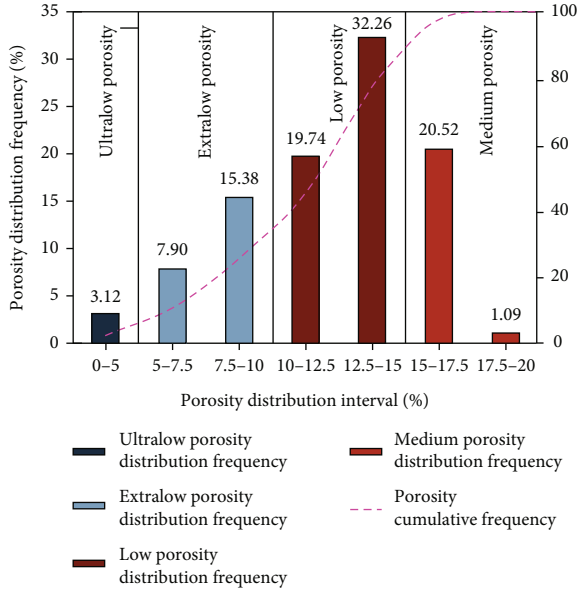
(a)
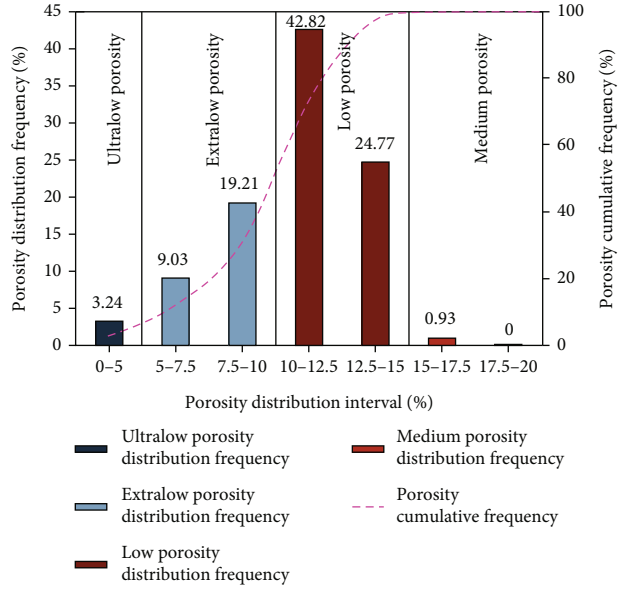
(b)

(c)
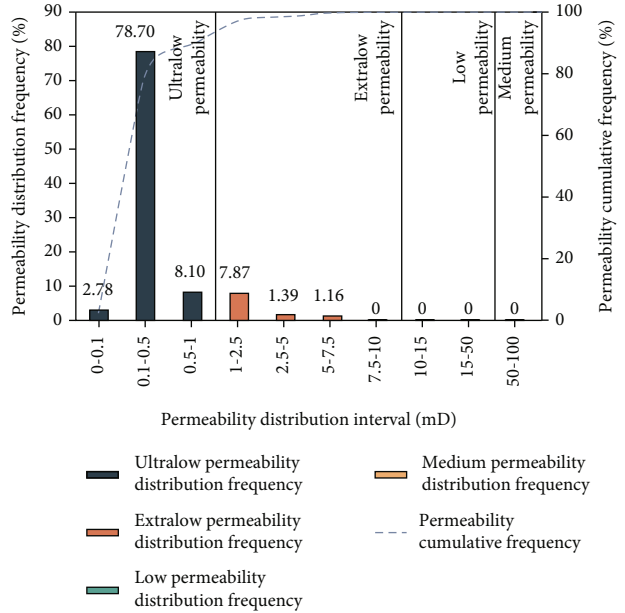
(d)

FIGURE 6: Distribution characteristics of core properties in the YPA and APA of the Chang 8_2 reservoir. (a) Distribution characteristics of reservoir porosity in the APA. (b) Distribution characteristics of reservoir porosity in the YPA. (c) Distribution characteristics of reservoir permeability in the APA. (d) Distribution characteristics of reservoir permeability in the YPA.

In general, the plane porosity in the APA is slightly higher than that in the YPA, and the plane porosity of the intergranular pores in the APA is significantly higher than that in the YPA. Moreover, the plane porosity of feldspar dissolution pores in the APA is lower than that in the YPA. In addition, compared with the YPA, the rock
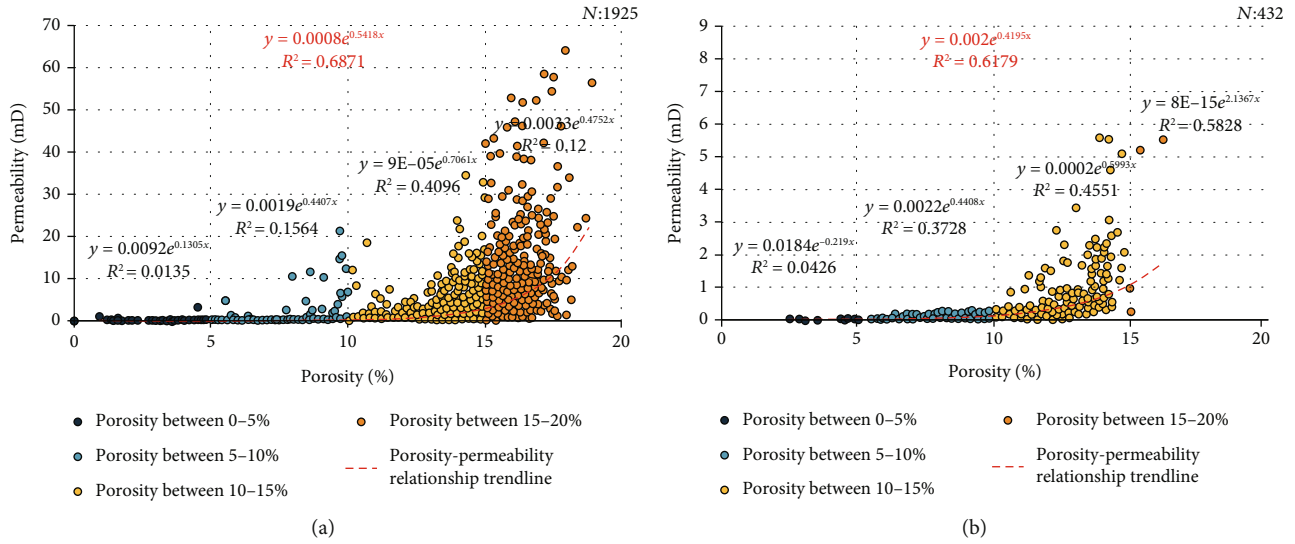
FIGURE 7: Difference in the correlation between porosity and permeability in the Chang 8_2 reservoir in the YPA and APA. (a) Correlation between the porosity and permeability of the APA reservoir. (b) Correlation between the porosity and permeability of the YPA reservoir.

fragment content in the APA is lower, but the degree of dissolution of rock fragment debris is higher (Figure 5(b)).

4.2. Reservoir Physical Properties

4.2.1. Characteristics of Porosity and Permeability Parameters.
The physical property data of core analyses from 2357 samples (from 53 wells) in the Chang 8_2 reservoir of the study area were organized. Although the YPA and APA are both low-porosity ultralow-permeability reservoirs, there are obvious differences in their physical properties.

The Chang 8_2 reservoir has porosities ranging from 0.92% to 18.89%, with an average of 11.88%, and permeabilities ranging from 0.002 to 64.267 mD, with an average of 2.997×10^{-3} um^2, and it is a low-porosity and ultralow-permeability reservoir. The comparison of the physical properties of the YPA and APA reservoirs shows that the average porosity of the APA reservoir is 12.14% and the average permeability is 3.573×10^{-3} um^2, which are much higher than the average porosity (10.71%) and the average permeability (0.431×10^{-3} um^2) of the YPA reservoir (Table 4).

The distribution histograms of the physical properties of the YPA and APA reservoirs were drawn (Figure 6). The frequency of the porosity distribution in the ultralow-porosity range of the APA reservoir is slightly lower than that in the YPA, and the porosity distribution frequency in the ultralow-porosity range is also slightly lower than that in the YPA. Among the distribution frequencies in the low-porosity range, the APA porosities are concentrated between 12.5% and 15%, while the YPA porosities are concentrated between 10% and 12.5%; the distribution frequency in the medium-porosity range is much higher in the APA than in the YPA, indicating that the great advantage of reservoir porosity in the APA comes from the relatively large pore area (Figures 6(a) and 6(b)).

In terms of permeability distribution frequency, the distribution frequency of reservoirs in the APA is much higher than that in the YPA in the range of $<0.1\,\mu\text{m}^3$, but the total ultralow-permeability range in the APA is much lower than that in the YPA. In the ultralow-permeability range, the APA still has a considerable distribution frequency (36.73%), but the YPA accounts for only 10.43% in this range, which is much lower than the APA. Even in the low and medium permeability ranges, the APA still has a certain distribution frequency, so the reason that the permeability in the YPA is much lower than that in the APA is that the proportion of the ultralow-permeability is too large, which seriously affects the reservoir permeability (Figures 6(c) and 6(d).

4.2.2. Physical Property Correlation Analysis.
According to the measured porosity and permeability parameters of the core physical properties, the correlation between porosity and permeability in the YPA and APA of the Chang 8_2 reservoir were analyzed (Figure 7).

According to the porosity limits of 0-5% (ultralow porosity), 5-10% (extralow porosity), 10-15% (low porosity), and 15-20% (medium porosity), the physical property correlation charts are divided into intervals. There is almost no correlation between the physical properties of the YPA and APA reservoirs in the ultralow-porosity interval, but after entering the ultralow-porosity interval, the correlation of the physical properties in the APA is significantly worse than that in the YPA (APA R^2: 0.1564 < YPA R^2: 0.3728).

Figure 7(a) shows that the existing samples in the APA ultralow-porosity interval have relatively high permeability, up to approximately 20 mD, while the permeability of the YPA reservoir in this interval is still poor. In the low-porosity interval, the physical property correlation in the YPA is slightly better than that in the APA, but Figure 7(b) shows that the local high permeability (<6 mD) is still much lower than that in the APA, indicating that the pore structure corresponding to the low-porosity interval
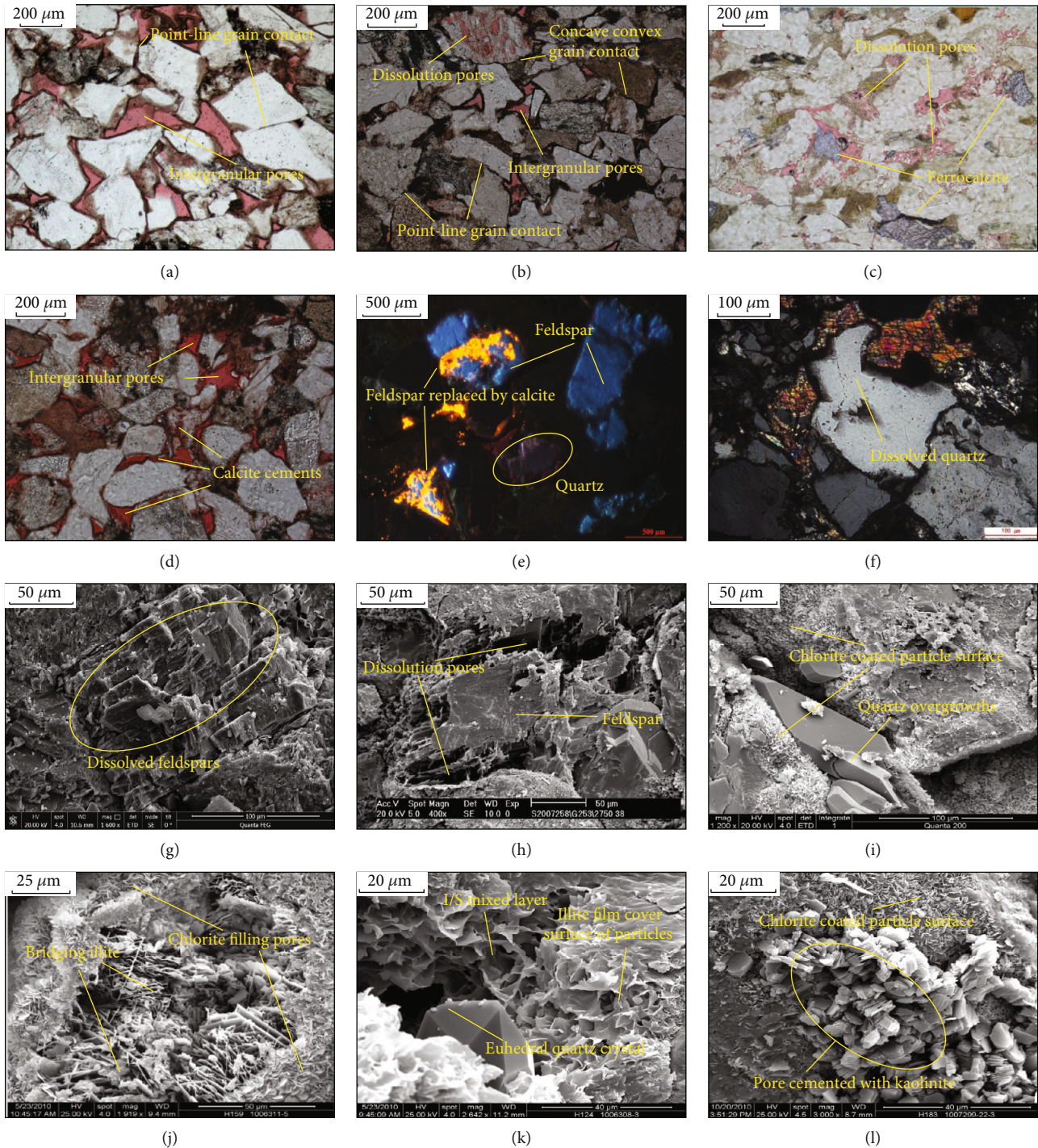
Figure 8: Comparison of different types of diagenesis between the YPA and APA Chang 8_2 reservoirs. Thin section photomicrographs, cathodoluminescence, and SEM images showing (a) APA, point-line grain contact; (b) YPA, point-line grain contact and concave-convex contact; (c) APA, ferrocalcite metasomatic feldspar; (d) YPA, calcite metasomatic feldspar; (e) APA, feldspar dissolved and replaced by calcite; (f) YPA, quartz dissolution; (g) APA, feldspar dissolution; (h) YPA, dissolved feldspar and dissolution pores; (i) APA, siliceous cementation and quartz overgrowth; (j) APA, illite bridging cemented filling pores; (k) YPA, illite and I/S mixed layer, siliceous cementation filling intergranular pores; and (l) YPA, chlorite coating, chlorite, and kaolinite filling dissolved pores.

in the YPA does not have good seepage capacity. In the medium-porosity interval, the correlation of APA samples is poor due to the surge in permeability, but the correlation indicates the characteristics of the strong seepage capacity in the APA when the porosity is good. Since the number of
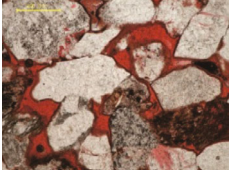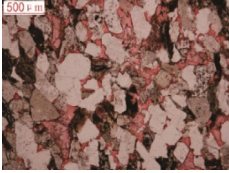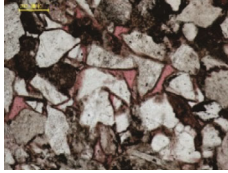
samples that can reach the medium-porosity interval is small in the YPA, the correlation is not convincing.

4.3. Differences in Diagenesis Types and Characteristics. According to the casting thin section, scanning electron

TABLE 5: Differences in the quantitative characterization of the densification process of the YPA and APA reservoirs.

Distribution	Value	Porosity %	Permeability ×10^{-3}μm^2	S_P	OPV %	VCR %	VCER %	VDR %	DC
YPA N:10	Max	13.75	0.68	1.23	41.36	83.25	48.66	85.21	0.12
	Min	3.21	0.01	1.12	39.84	31.64	15.68	11.64	0
	Avg	8.31	0.21	1.17	39.24	56.71	30.07	43.78	0.05
APA N:10	Max	16.99	7.5	1.21	41.36	82.35	37.53	78.57	0.15
	Min	6.28	0.04	1.12	39.53	53.30	12.35	0	0
	Avg	10.86	1.51	1.14	41.13	58.18	22.54	28.83	0.04

TABLE 6: Classification of diagenetic facies types and microscopic characteristic parameters in the study area.

Type	I	II	III	IV
Microscope				
Kaolinite %	0-2 (0.13)	0-4 (1.67)	0-3 (0.64)	0-8 (3.14)
Illite %	0-4.5 (1.06)	1-7 (3.58)	0-5 (1.19)	0.2-4.8 (2.05)
Chlorite %	1.5-13.2 (5.27)	0.5-3 (1.63)	1-9 (5.35)	0.3-7.2 (2.60)
Carbonate %	0-6 (2.31)	0-17 (3.33)	0.2-20 (5.51)	0-39 (11.56)
Silica %	0.5-3.5 (1.30)	0.5-5 (2.56)	0.3-5.2 (2.29)	0-2.5 (1.14)
Intergranular pores %	1-12 (6.02)	0-6 (1.93)	0-4.5 (1.32)	0-0.6 (0.30)
Dissolution pores %	0-4 (1.19)	0-4.5 (1.51)	0.2-1.5 (0.76)	0-0.7 (0.17)
Plane porosity%	1-14 (7.02)	0-7 (2.82)	0.3-4.8 (1.99)	0-1.7 (0.44)
Average pore size μm	20-210 (75.10)	5-70 (36.43)	10-90 (35.00)	5-20 (16.67)

Note: Values in parentheses are average values.

microscope, and typical cathodoluminescence sample observations, the diagenesis types in the YPA and APA are mainly compaction, metasomatism, dissolution, and cementation (Figure 8).

The compaction in the YPA and APA is similar, and point-line contacts are dominant, but the compaction in the YPA is stronger, and concave-convex contacts are locally visible (Figures 8(a) and 8(b)). Metasomatism is mainly caused by carbonate minerals replacing feldspar (Figures 8(c)–8(e)), and clay minerals may occasionally replace quartz or feldspar. After APA metasomatism, intergranular pores and dissolution pores are still present, but the pore filling degree is higher after YPA metasomatism. The dissolution is dominated by feldspar dissolution, with occasional quartz dissolution and rock fragment dissolution [45] (Figures 8(e)–8(h). The degree of dissolution in the APA is higher, but dissolution is more important for the development of pores in the YPA. The cementation in the YPA and APA is dominated by clay minerals, carbonates, and siliceous cementing and filling pores (Figures 8(i)–8(l)), but the pore structure in the YPA is relatively small, indicating that cementation has a more significant pore-reducing effect in the YPA.

4.4. Reservoir Densification Characterization Results. Table 5 shows the quantitative characterization and calculation parameters of the densification process of a total of 20 samples from the YPA and APA reservoirs.

The average selection coefficient S_P of the APA is 1.17, while that of the YPA is 1.14, indicating that the YPA has better selection. The average original pore volume in the APA is 41.13% and that in the YPA is 39.24%, reflecting larger pores in the APA. The comparison of the visual compaction rate shows that the APA is more affected by compaction than the YPA. The comparison of the visual cementation rate shows that the YPA is more affected by cementation than the APA. In addition, the visual dissolution rate indicates that the YPA is more affected by dissolution than the APA. In addition, the diagenetic coefficient indicates that the YPA is more affected by diagenesis than the APA.

4.5. Diagenetic Facies

4.5.1. Types and Characteristics of Diagenetic Facies. Since the diagenetic evolutionary patterns of the YPA and APA reservoirs are consistent and the overall diagenesis types are not very different, to establish a unified reservoir evaluation standard, this paper integrates the diagenetic characteristics of the YPA and APA reservoirs. Four types of dominant diagenetic facies were identified after the whole area was screened based on the principle of combining the
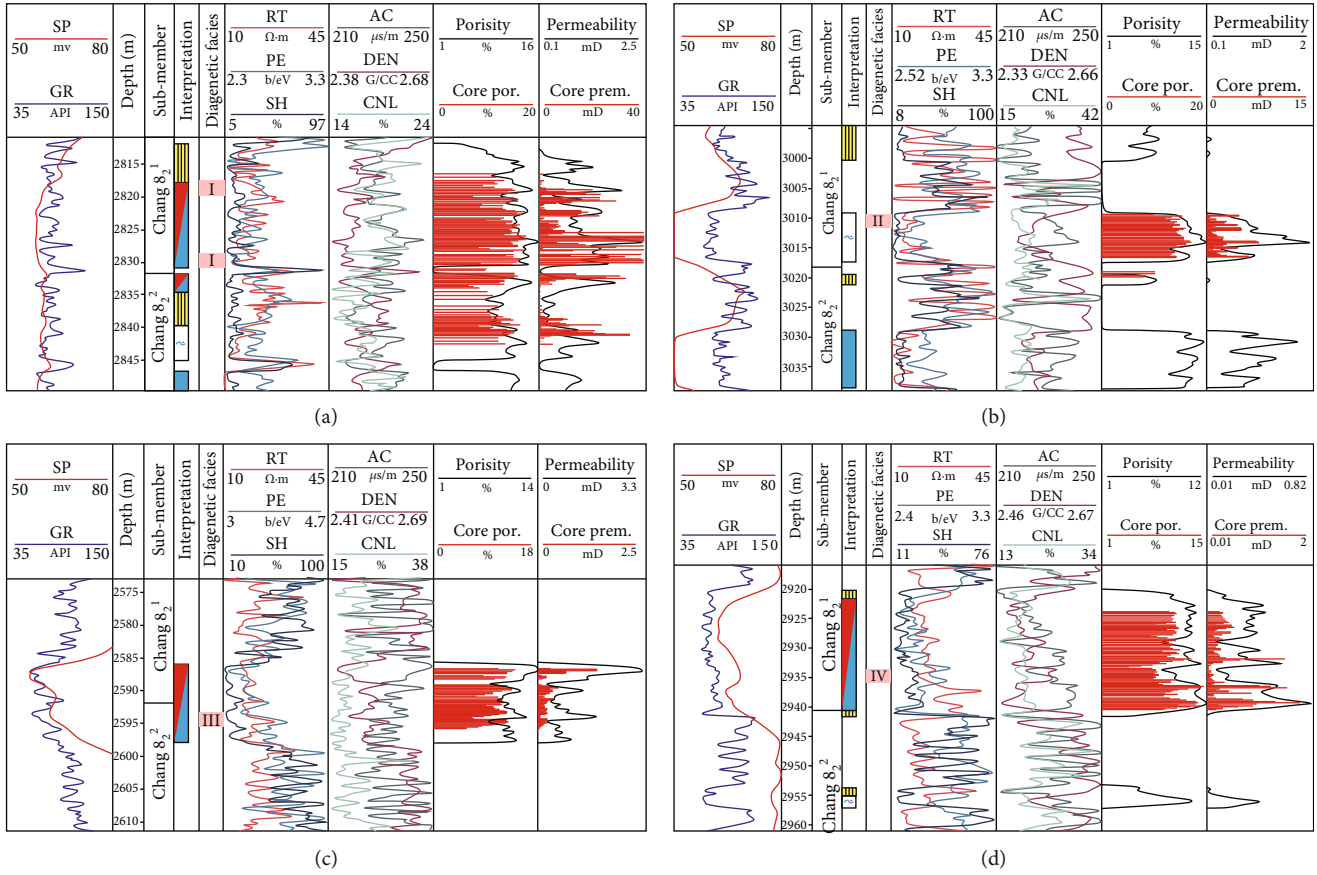
(a)

(b)

(c)

(d)

FIGURE 9: Characteristics of the four types of diagenetic facies logging curves identified by lithoelectric calibration in the Chang 8_2 reservoir in the study area. (a) Type I: chlorite coating residual intergranular pore diagenetic facies; (b) type II: illite-siliceous cemented dissolved pore diagenetic facies; (c) type III: chlorite-filled-carbonate cemented microporous diagenetic facies; (d) type IV: carbonate cemented, compacted, and dense diagenetic facies.

TABLE 7: Logging characterization of four types of diagenetic facies in the YPA and APA.

Diagenetic facies	SP mv	GR API	RT $\Omega \cdot m$	PE b/eV	SH %	AC $\mu s/m$	DEN g/cm^3	CNL %	POR %	PERM mD
Type I	58.96	72.48	25.68	2.66	12.93	243.05	2.44	19.52	13.12	1.69
Type II	48.66	72.96	21.42	2.67	15.32	237.57	2.49	19.77	11.16	0.95
Type III	62.04	73.22	17.66	2.71	15.98	234.29	2.50	17.19	8.26	0.51
Type IV	68.26	80.73	15.37	2.73	25.94	228.45	2.56	18.38	5.24	0.18

characteristic particle type, characteristic cement type, and main diagenesis (Table 6).

Among them, type I represents chlorite lining-residual intergranular pore diagenetic facies, and type II represents illite-siliceous cemented dissolution pore diagenetic facies. Type III represents chlorite filling-carbonate cemented micropore diagenetic facies. In addition, type IV represents carbonate cementation-compaction compact diagenetic facies.

4.5.2. Logging Calibration of Diagenetic Facies. The differences in the parameters of the logging curve can effectively characterize its development characteristics; then, the diagenetic facies of noncored wells can be calibrated after the whole area is extended (Figure 9).

The logging identification results of the four types of diagenetic facies are shown in Table 7.

(1) Type I

Well H390 at 2830.84 m and 2819.94 m is taken as an example (Figure 10(a). A high AC represents a higher primary pore content, and a low DEN indicates larger pores. A lower CNL indicates a lower hydrogen content, and a lower RT represents the adsorption of radioactive substances by chlorite. The PE is relatively low, the gap is not large, and the porosity and permeability explained by electrical measurements are relatively large, which are usually developed at the bottom of underwater distributary channels and the middle and lower parts of estuary bars.
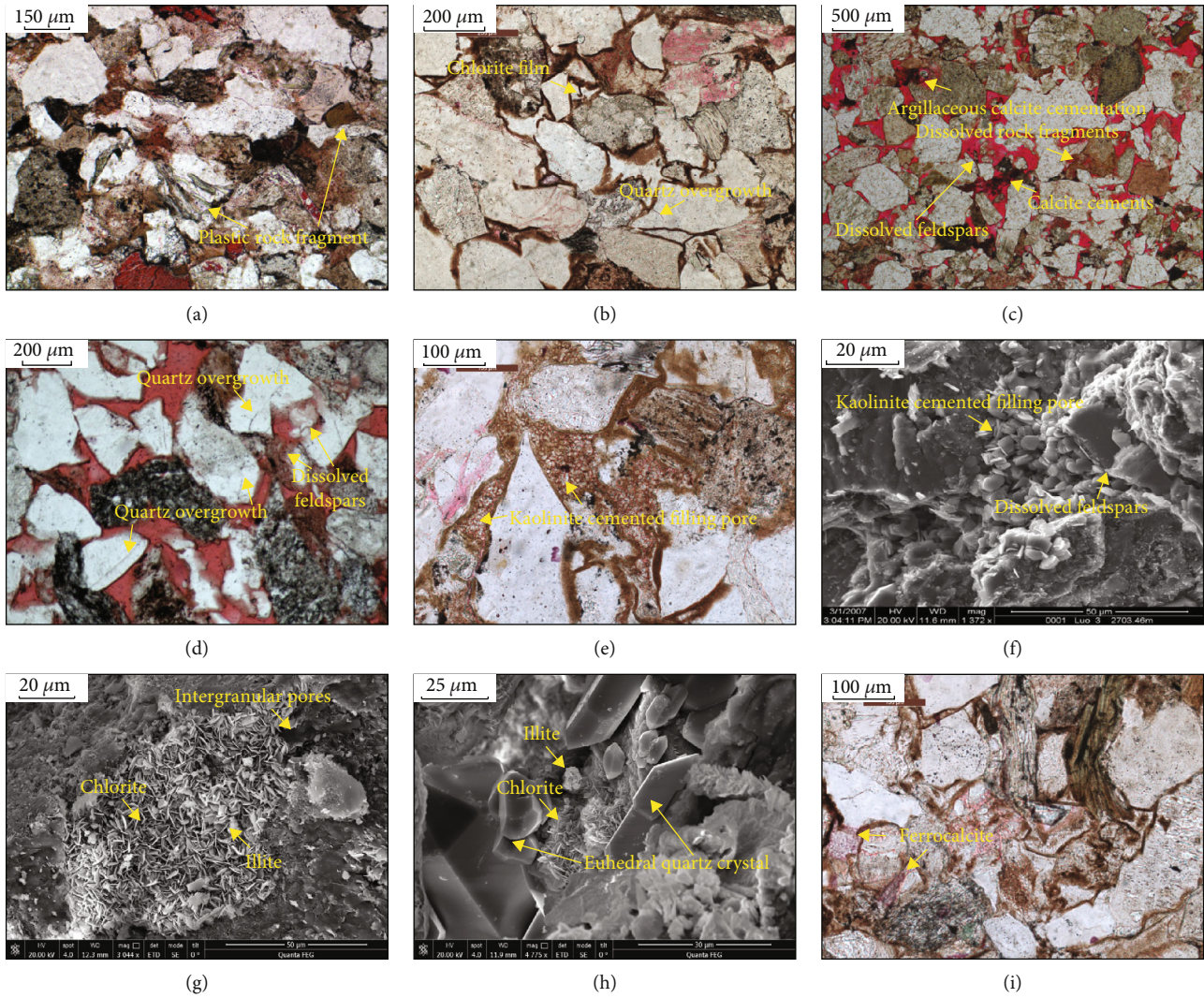
Figure 10: Factors for the identification of a typical diagenetic sequence. Thin section photomicrographs and SEM images show the following: (a) YPA: compaction results in the tight fitting of particles and compression of cuttings; (b) APA: chlorite film developed earlier than quartz overgrowths; (c) APA: in the early stage of calcite cementation development, the grains were mainly in point contact, and a chlorite coating existed around the grains; (d) APA: quartz overgrowths occurred earlier than the dissolution of feldspar and rock fragments; (e) APA: feldspar and rock fragments are dissolved and filled with kaolinite; (f) YPA: when kaolinite fills the dissolution pores, illite and chlorite have not yet been filled; (g) APA: the pores are filled with chlorite and a small amount of illite; (h) APA: euhedral quartz fills in later than chlorite and illite; and (i) APA: late ferrocalcite cementation.

Table 8: Four types of diagenetic facies classification function coefficients.

$F(I) = 32.915 \times SP - 27.971 \times GR + 191.106 \times RT - 487.061 \times PE + 57.838 \times SH + 93.48 \times AC + 132.155 \times CNL + 13384.491$	(1.9)
$F(II) = 31.491 \times SP - 26.888 \times GR + 184.38 \times RT - 470.384 \times PE + 55.039 \times SH + 90.345 \times AC + 126.619 \times CNL - 12458.307$	(1.10)
$F(III) = 33.292 \times SP - 28.156 \times GR + 193.961 \times RT - 494.024 \times PE + 58.139 \times SH + 95.03 \times AC + 132.356 \times CNL - 13793.15$	(1.11)
$F(IV) = 34.716 \times SP - 29.205 \times GR + 198.682 \times RT - 504.168 \times PE + 62.214 \times SH + 96.67 \times AC + 139.406 \times CNL - 14455.288$	(1.12)

(2) Type II

Well H468 at 3011.63 m is taken as an example (Figure 10(b)). Because it is mostly developed in the upper part of the underwater distributary channel, the muddy sediment is enhanced, and the radioactive content is increased, so the GR is relatively high. The occurrence of siliceous cementation resulted in lower RT and moderately high DEN. Moreover, the moderately low AC is also caused by the development of siliceous cementation, and the occurrence of dissolution makes the CNL moderately high.

(3) Type III

Well H323 at 2594.3 m is taken as an example (Figure 10(c)). The higher SP and GR indicate the higher

content of argillaceous sediments. A moderately low RT indicates that the clay minerals adsorbed radioactive substances and the volume of bound water is increased, resulting in a high hydrogen content. The overall trend of CNL is moderate, the larger PE reflects the change in lithology, and the porosity reduction caused by cementation leads to the decrease in the explained physical properties again, which is usually located in the lower part of the estuary bar.

(4) Type IV

Well H497 at 2935.02 m is taken as an example (Figure 10(d)). The development location is similar to the calcareous interlayer, which is usually located in the upper part of the underwater distributary channel, mostly in an evaporative environment. SP and GR are moderately high, AC easily forms an aiguille, and PE is moderately high. Carbonate cementation increases RT and lowers CNL, and compaction cementation leads to higher density [48], so DEN is higher, and the physical properties explained by electrical measurements are smaller.

4.5.3. Establishment of the Diagenetic Facies Discriminant Function by Cluster Analysis. After the first collinear diagnosis, the dependent parameter types, namely, DEN, POR, and PREM, are removed, and the results of the second collinear diagnosis meet the requirements of this paper. Based on the statistical standard of a VIF of less than 10, there is no significant multicollinearity among the remaining logging curves, including SP, GR, RT, PE, SH, AC, and CNL [43, 48].

The Fisher discriminant function was used to establish the relational formula of each diagenetic facies type (Table 8).

Discriminant analysis shows that the group centroids of various diagenetic facies are distributed farther (Figure 11).

5. Discussion

5.1. Relationship between the Clay Mineral Content and Physical Properties. According to the correlation diagram between different types of clay minerals and physical properties, the following findings are obtained (Figure 12).

The illite content in the APA is negatively correlated with the physical properties of the reservoir. The surface leaf-shaped or hairline-shaped illite fills the intergranular pores significantly, thereby dividing the pores, increasing the tortuosity, and blocking pore throats [48] (Figures 12(a) and 12(b)).

The I/S mixed layer is related to the temperature and pressure of the burial depth and plays a role in reducing the physical properties of the reservoir [48]. It is speculated that the honeycomb-like I/S mixed layer on the grain surface or between the grains blocks the pore throats to some extent [9] (Figures 12(c) and 12(d)).

The kaolinite in the YPA and APA has a poor correlation with the reservoir physical properties, only a weak negative correlation, and appears in the form of pore filling [11]. In particular, it has a greater impact on smaller throats, so the physical properties of reservoirs in the YPA are also
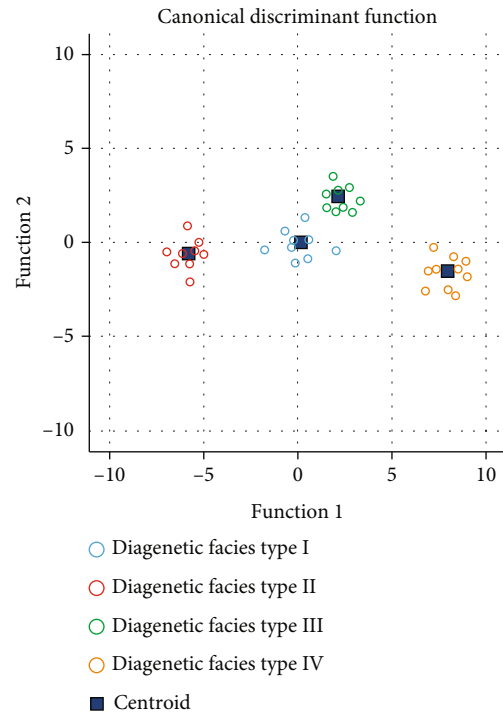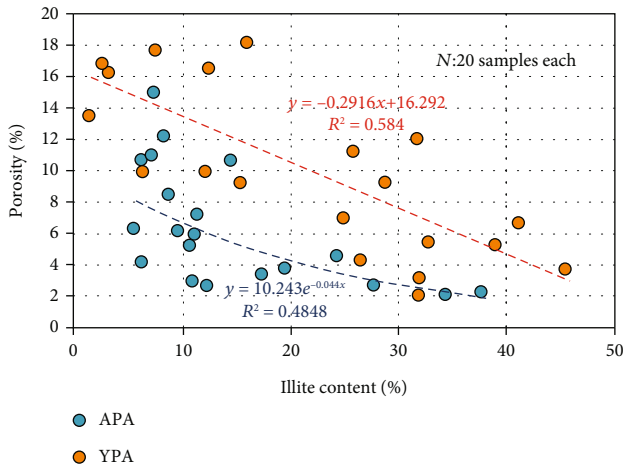
FIGURE 11: Distribution of the centroids of the four types of diagenetic facies groups.

more significantly affected by the kaolinite content than in the APA (Figures 12(e) and 12(f)).
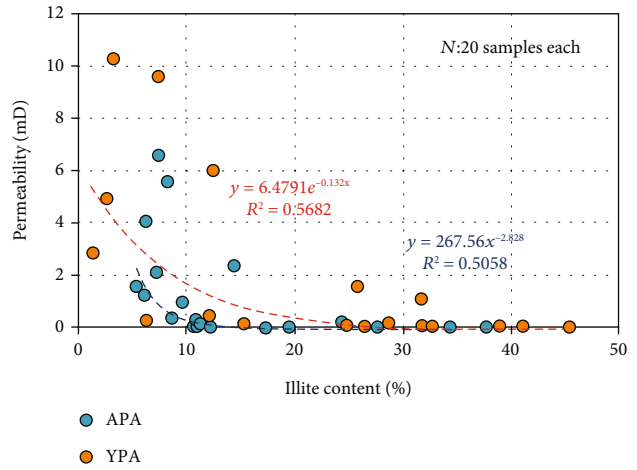
The APA chlorite is positively correlated with physical properties. Because chlorite in the study area mostly appears in the form of pore liner or grain surface film, which is cone-shaped and has a strong constructive effect on the reservoir, the physical properties increase significantly with increasing chlorite content. However, because the average chlorite content in the YPA is higher than that in the APA, the degree of pore filling is also higher than that in the APA, which is also the reason why the physical properties of the reservoir in the YPA are worse than those in the APA (Figures 12(g) and 12(h)). More importantly, affected by structural differences, the APA located on the edge of the basin is more susceptible to structural compression, while the YPA located in the interior of the basin is less compressed, so differential compaction is also one of the reasons for the relatively low degree of compaction of YPA.

5.2. Different Effects of Diagenesis on Reservoir Densification. Based on the calculation results of reservoir densification, the correlations between the visual compaction rate, visual cementation rate, visual dissolution rate, and diagenesis coefficient and physical properties were plotted [13] (Figure 13).
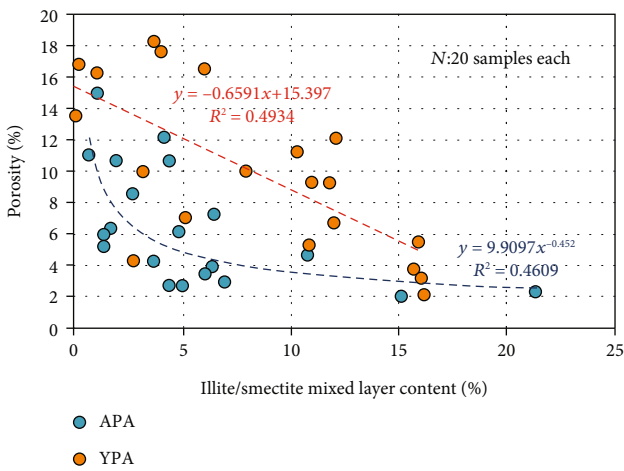
A comparison reveals that the visual compaction rate and physical properties have a good negative correlation. However, the negative correlation between the visual compaction rate and physical properties in the APA is significantly stronger than that in the YPA, indicating that the better pore structure in the APA is more susceptible to compaction than that in the YPA, resulting in a significant porosity reduction effect (Figures 13(a) and 13(b)).
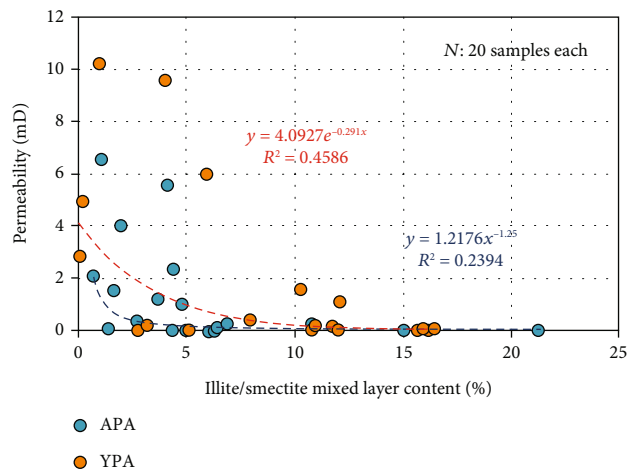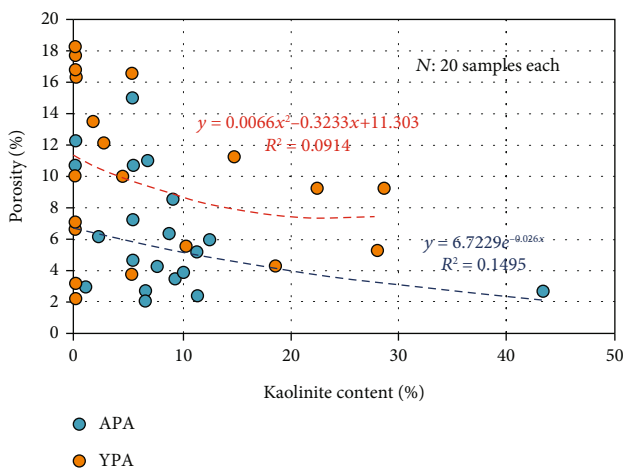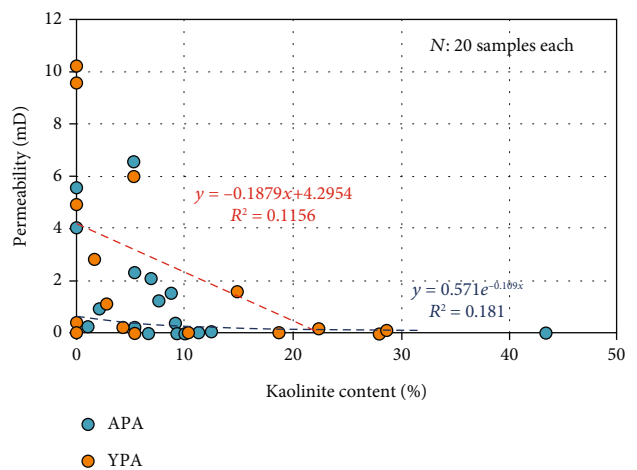
(a)

(b)

(c)

(d)

(e)

(f)

Figure 12: Continued.

$y = 0.0015x^2 - 0.0201x + 4.6979$
$R^2 = 0.5652$

$y = 0.004x^2 - 0.3404x + 9.0093$
$R^2 = 0.5113$

N:20 samples each

APA
YPA

(g)

$y = 0.0029e^{0.0769x}$
$R^2 = 0.558$

$y = 0.008e^{0.0785x}$
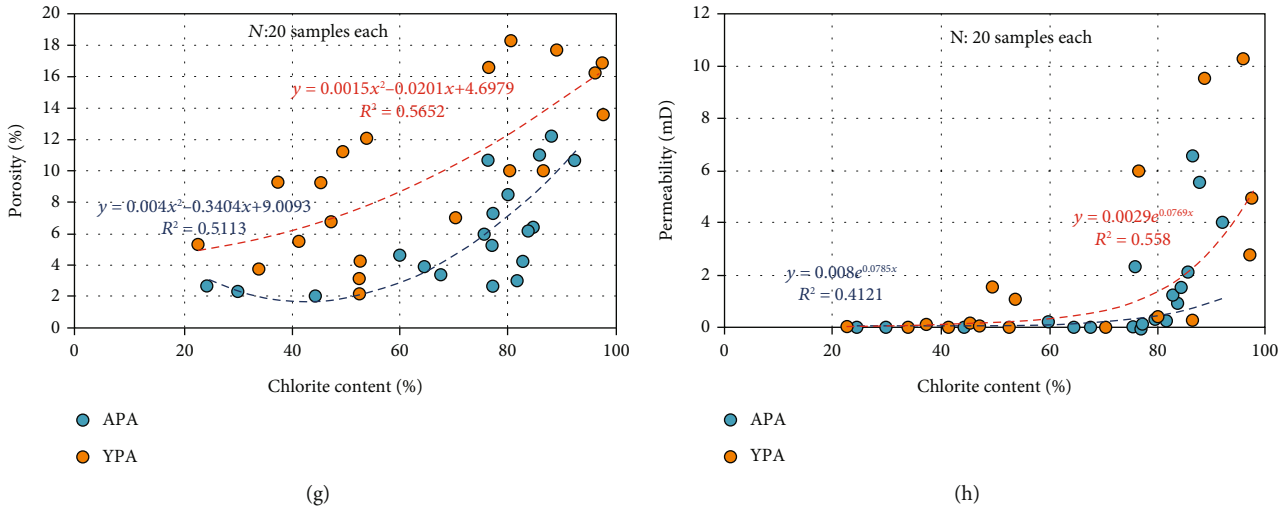$R^2 = 0.4121$

N: 20 samples each

APA
YPA

(h)

FIGURE 12: Relationship between different types of clay minerals and physical properties in the YPA and APA. (a) Difference in the correlation between the illite content and porosity. (b) Difference in the correlation between the illite content and permeability. (c) Difference in the correlation between the illite/smectite mixed layer content and porosity. (d) Difference in the correlation between the illite/smectite mixed layer content and permeability. (e) Difference in the correlation between the kaolinite content and porosity. (f) Difference in the correlation between the kaolinite content and permeability. (g) Difference in the correlation between the chlorite content and porosity. (h) Difference in the correlation between the chlorite content and permeability.

The visual cementation rate is also negatively correlated with the physical properties, but the correlation between the visual cementation rate and the physical properties of YPA reservoirs is significantly stronger than that between the visual cementation rate and the physical properties of the APA, indicating that those different types of cementations damage YPA reservoirs (Figures 13(c) and 13(d)).

Visual dissolution rates are all positively correlated with physical properties [49], but the correlation between visual dissolution rates and reservoirs in the YPA is stronger than that in the APA, indicating that the effect of dissolution on the reservoirs in the YPA is greater than that in the APA. Therefore, the improvement in the physical properties of the YPA reservoir is more dependent on the generation of dissolution pores (Figures 13(e) and 13(f)).

The diagenetic coefficients are significantly positively correlated with the YPA and APA reservoirs, but the correlation between YPA reservoirs and the diagenetic coefficients is significantly better than that in the APA, indicating that the formation, development, evolution, and diagenesis of YPA reservoirs are more closely related than those in the APA (Figures 13(a) and 13(h)). It is speculated that the relatively poorer pore structure is more dependent on diagenetic transformation.

5.3. Differences in the Diagenetic Stage and Reservoir Pore Evolution.

The typical diagenetic sequences in the YPA and APA are similar and are followed by early mechanical compaction, chlorite clay film, early argillaceous calcite basement cementation, secondary overgrowth of quartz, dissolution of feldspar and rock fragments, authigenic kaolinite cementation, pore filling illite and chlorite, authigenic quartz cementation, late ferrocalcite cementation, and metasomatism.

The diagenetic stages are classified as follows (Figure 10). Reservoirs in the YPA and APA are moderately compacted,

the particle contacts are mainly point-line, while point-like and concave-convex contacts are also visible, and the physical properties are poor. The overall tightness of the reservoir is relatively high, and the cementation of calcareous and clay minerals is visible. Quartz secondary overgrowths and feldspar overgrowths are visible, and microcrystalline quartz filling pores is visible in many samples. Carbonate cementation is common with embedded calcite or ferrocalcite cement, and small amounts of micrite and bright dolomite are visible in the photos. Chlorite and illite cementation are common, and there are few mixed I/S layers. The I/S mixed layer ratios are between 5% and 30%, indicating an ordered mixed layer. The early chlorite is dominated by pore lining, and cone-shaped and pompom-like chlorite cementations are visible in the late stage. Some illite and chlorite are mixed, thereby filling the pores [50], or cemented along the edge of the grain ring, and kaolinite fills the pores in the shapes of book pages and worms [13]. Secondary pores are relatively developed, and cracks are visible. In addition, residual asphalt is visible in the pores, and the evolution of organic matter has entered the mature stage [51].

The diagenetic stage was identified in combination with paleogeothermal temperatures (100-130°C), organic matter ($R_o = 0.88\%$) [10, 30], the sandstone consolidation degree, the authigenic mineral assemblage, dissolution, the particle contact relationship, the diagenetic environment, and the pore type, and the pore evolution was analyzed according to the process of reservoir densification (Figure 14).

A comparison reveals that the diagenetic stages reached by the reservoirs in the YPA and APA are still different. According to the classification standard of clastic rock diagenetic stages [52], it is believed that the APA reservoir is mainly in middle diagenetic stage A, while the YPA reservoir has reached middle diagenetic stage A or middle diagenetic stage B locally.
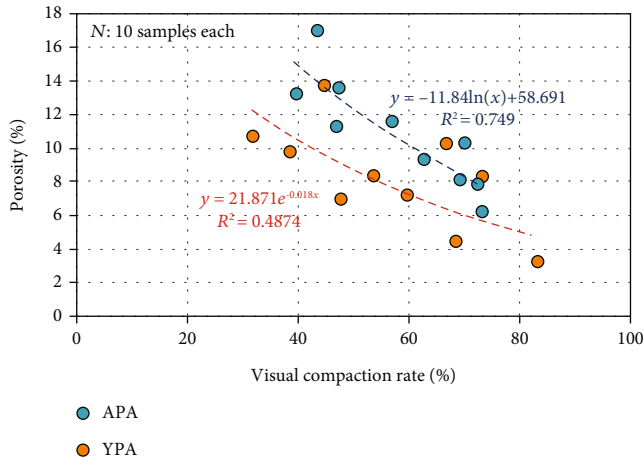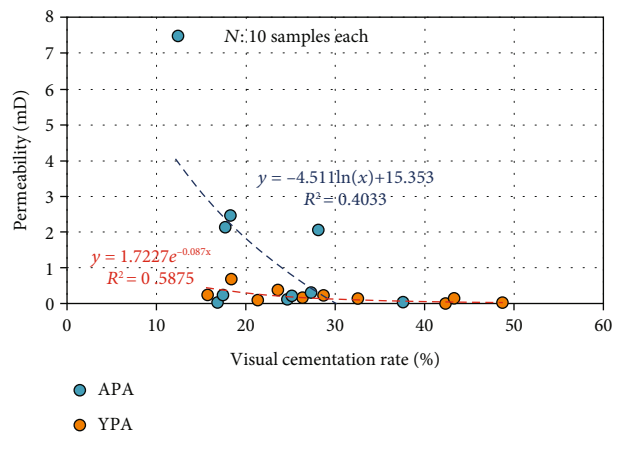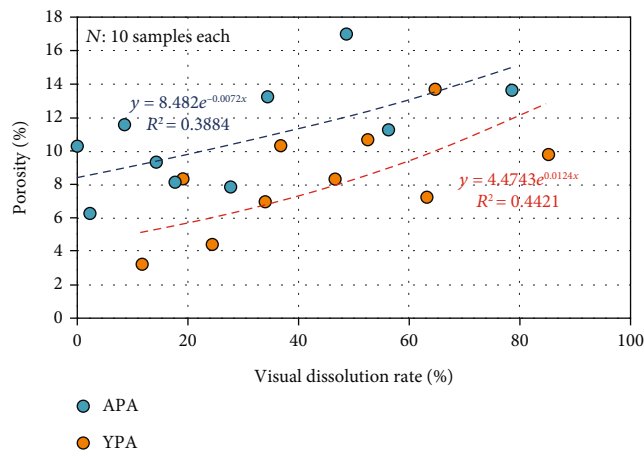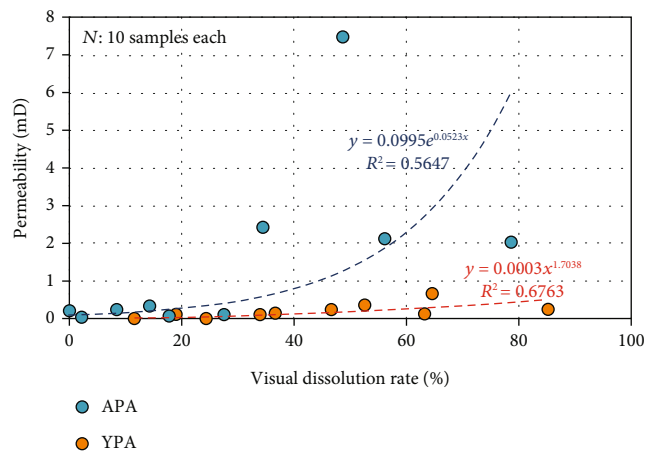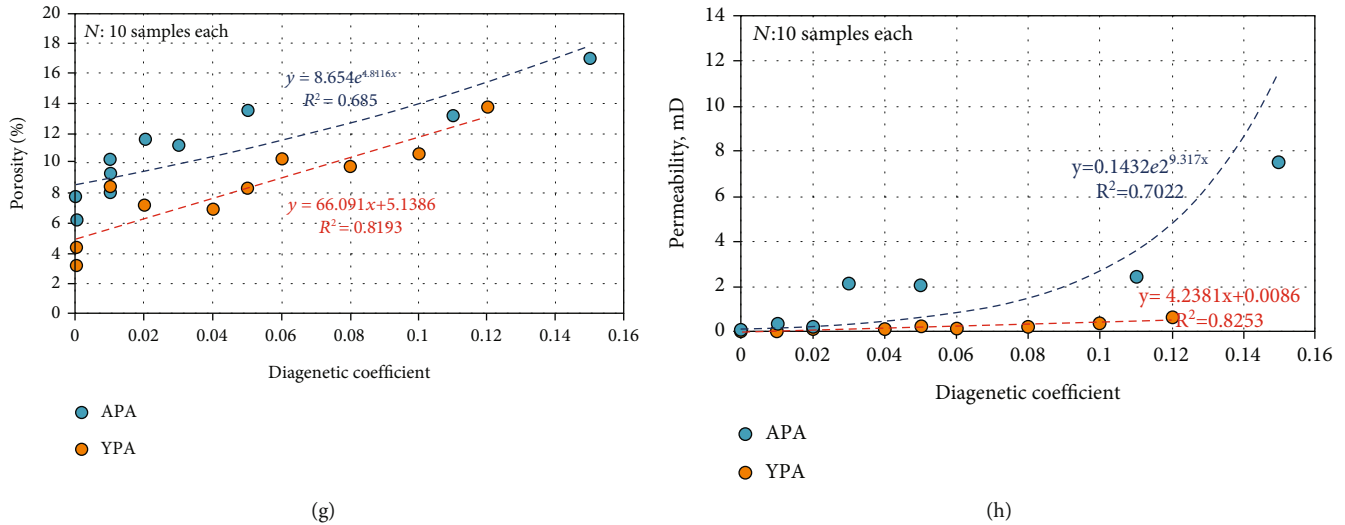
(a)
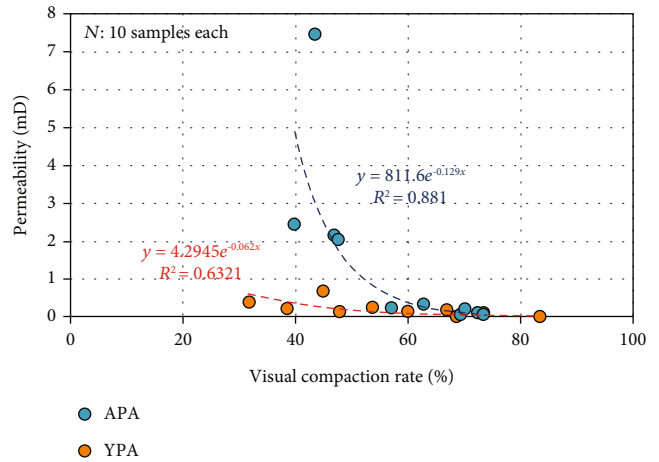
(b)
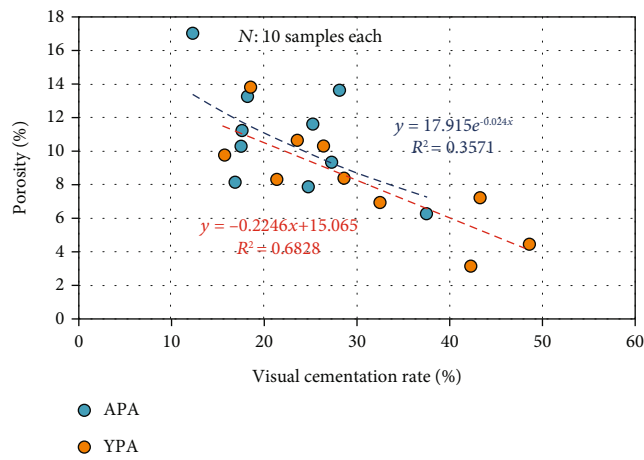
(c)

(d)

(e)

(f)

Figure 13: Continued.

(g)

(h)

FIGURE 13: Correlation between diagenetic densification parameters and the physical properties of the YPA and APA Chang 8_2 reservoirs. (a) Correlation between the visual compaction rate and porosity; (b) correlation between the visual compaction rate and permeability; (c) correlation between the visual cementation rate and porosity; (d) correlation between the visual cementation rate and permeability; (e) correlation between the visual dissolution rate and porosity; (f) correlation between the visual dissolution rate and permeability; (g) correlation between the diagenetic coefficient and porosity; and (h) correlation between the diagenetic coefficient and permeability.

In early diagenetic stage A, the basin was in a stable subsidence stage, compaction and cementation were carried out at the same time, and the early cement chlorite film began to form. Due to the high chlorite content in the YPA, the chlorite film has a better anticompaction effect, so the porosity in the YPA was slightly lower than that in the APA after compaction. Carbonate cement began to precipitate in a weakly alkaline environment, and micrite calcite cements began to form [13].

In early diagenetic stage B, the compaction was enhanced, the clastic particles were arranged in a directional manner, and the primary and secondary overgrowths of quartz were produced. As hydrocarbon filling began, small amounts of feldspar and rock fragments began to dissolve, and kaolinite appeared.

In middle diagenetic stage A, compaction and kaolinite and siliceous cementation continued. After a large number of hydrocarbons were charged, dissolution became dominant, the storage space was improved, and strong dissolution led to the transformation of kaolinite into illite. The proportion of illite in the I/S mixed layer increased. In addition, the massive formation of siliceous chlorite resulted in secondary overgrowths, and the transformed authigenic chlorite began to fill the pores.

The diagenetic evolution stages in the YPA and APA reservoirs are relatively consistent, and the differences in porosity evolution are caused by different mineral contents. The occurrence of a large amount of dissolution has significantly improved the YPA reservoir, resulting in a relatively large porosity recovery. After middle diagenetic stage A, the diagenetic stage of the APA reservoir was almost stagnant, and according to the X-diffraction results, illite accounted for less than 85% of the I/S mixed layer. The YPA reservoir gradually entered middle diagenetic stage B, and after the diagenetic environment changed to alkaline, middle and late

cementation began to occur. Ferrocalcite, illite, and quartz continued to form third-level secondary growth, destroying the pore throat structure and resulting in a larger decline in reservoir porosity in the YPA than in the APA. According to the X-diffraction results, illite accounts for more than 85% of the I/S mixed layers in the YPA, indicating middle diagenetic stage B.

There are also differences in the porosity evolution process of the YPA and APA reservoirs under the influence of diagenesis. The initial porosity in the APA was relatively large, but after compaction, the APA became only slightly larger than the YPA. After early cementation, the YPA was significantly affected, and the porosity decreased rapidly. However, after strong dissolution, the porosity in the YPA increased considerably and was only slightly lower than that in the APA. Since the YPA reservoir is more sensitive to cementation, the APA retains more porosity after experiencing middle and late cementation.

5.4. Relationship between the Diagenetic Facies Distribution and Reservoir Development. According to the diagenetic facies logging identification results, the plane distribution prediction figure of the four types of diagenetic facies in the Chang 8_2 reservoir was drawn (Figure 15).

Clearly, the distribution area of type I diagenetic facies in the APA reservoir is wider than that in the YPA (25.3% > 17.9%), indicating that the intergranular pores are more developed in the APA. However, the distribution of type II diagenetic facies in the APA is slightly lower than that in the YPA (21.3% < 22.1%), which indicates that the development degree of illite and siliceous cement in the APA is lower than that in the YPA and the degree of dissolution in the APA is lower than that in the YPA. The distribution range of type III diagenetic facies in the YPA is larger than that in the APA, reflecting that the YPA is more
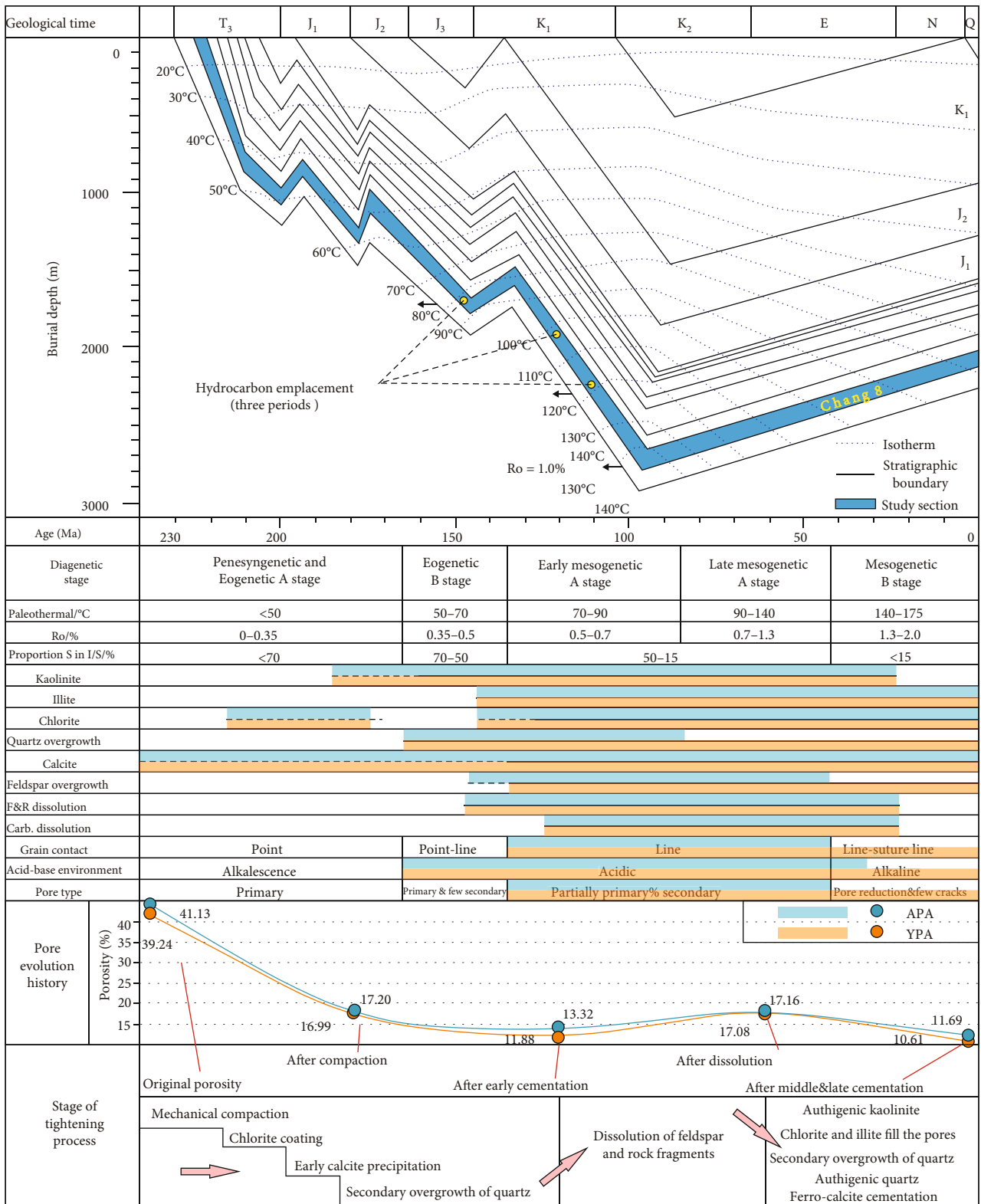
Figure 14: Differences in diagenetic stages and porosity evolution between the YPA and APA of the Chang 8$_2$ reservoir (modified from [10, 16]).

significantly filled with chlorite and cemented by carbonate. In addition, the distribution range of type IV diagenetic facies in the YPA is also slightly larger than that in the APA, indicating that the pore structure in the YPA is more dense, resulting in worse physical properties. In general, the APA contains more of type I and less of type IV, and
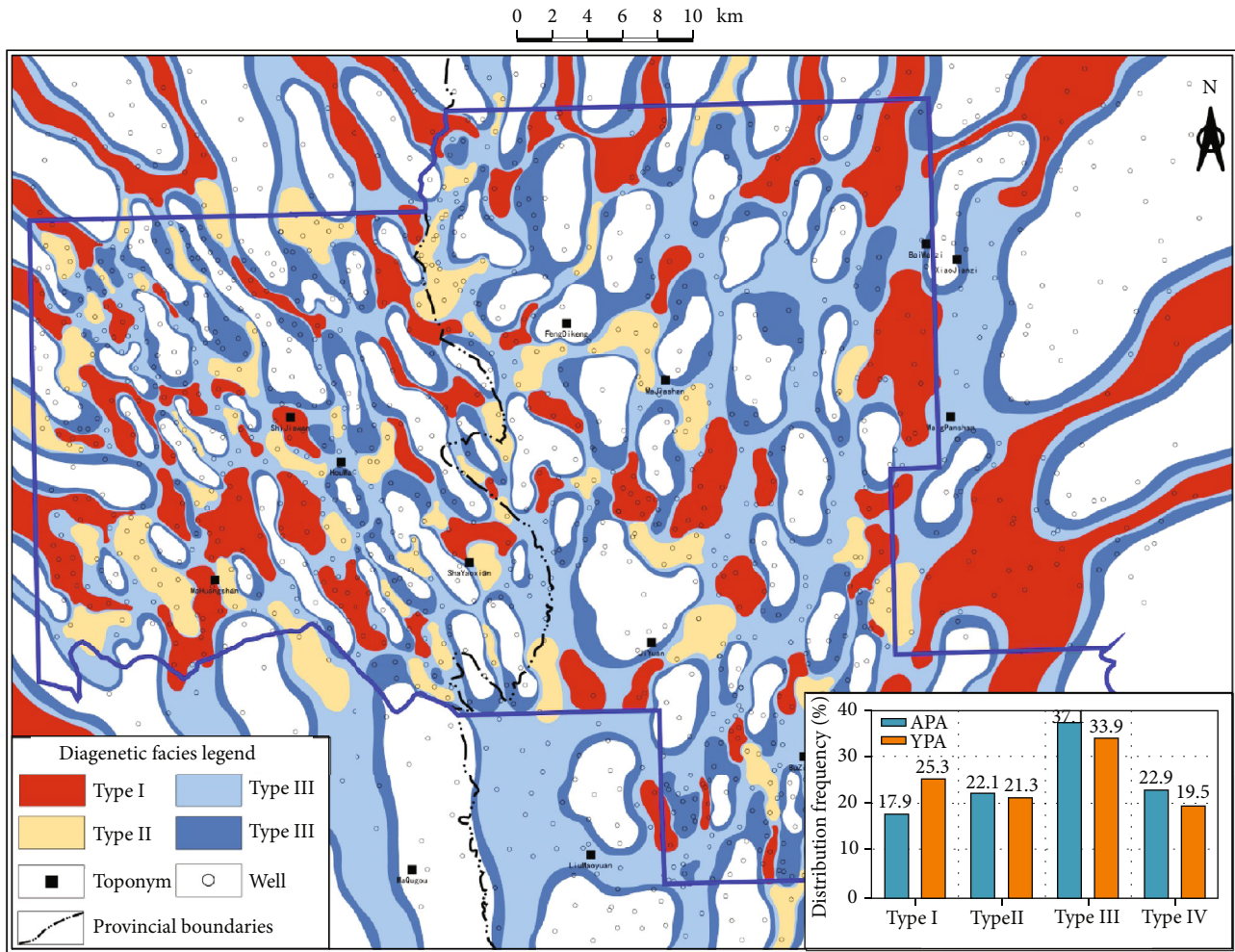
FIGURE 15: Prediction of the plane distribution of diagenetic facies in the Chang 8_2 reservoir in the YPA and APA.

the developed reservoir conditions are better than those in the YPA, with larger pore structures.

5.5. Differences in Reservoir Formation Mechanisms

5.5.1. Differences in Sedimentation. The Chang 8_2 submember in the study area developed shallow-water delta deposits, so the reservoirs are mainly underwater distributary channel facies [5, 9]. When the rivers met, the hydrodynamic effect was strong, relatively large particles were deposited to retain a relatively large pore space [12, 17], and the overall physical properties are relatively high. Conversely, when the hydrodynamic force was relatively weak on the flanks of the channel or in the interdistributary bay, the sedimentary particles were relatively small, and the corresponding pore space is also smaller [53]. The reservoir in the APA is closer to the provenance in the northwest, so the sedimentary hydrodynamics are generally stronger and the grain size is larger than that in the YPA [5]. However, at the same time, the sorting is also less than that in the YPA, which has experienced distant provenance deposition. Therefore, the underwater distributary channel deposits in the APA are more developed and distributed more widely than those in the YPA, which directly indicates that the foundation for the

formation of reservoirs in the APA is better than that in the YPA.

5.5.2. Differences in the Mineral Content. Compared with the YPA, the APA is closer to the provenance, and the quartz content is relatively low, so the compaction resistance is slightly lower than that of the YPA [16]. The feldspar content in the APA is slightly higher than that in the YPA, which can provide more matrix for dissolution and the basis for clay mineral transformation. However, the feldspar interstitial filling is also higher than that in the YPA, and the plugging of the pore structure is relatively strong, so the effect of the feldspar content on reservoir formation is complicated [9]. The carbonate interstitial content in the APA is slightly higher than that in the YPA, and the damage to the pores is more significant; however, the primary intergranular pore structure in the APA is much better than that in the YPA, and the impact of carbonate interstitial filling has difficulty causing a significant decrease in the physical properties of the reservoir in the APA.

The clay mineral content has a greater impact on the reservoir, and the I/S mixed layer content in the APA is higher than that in the YPA. However, as visible under the
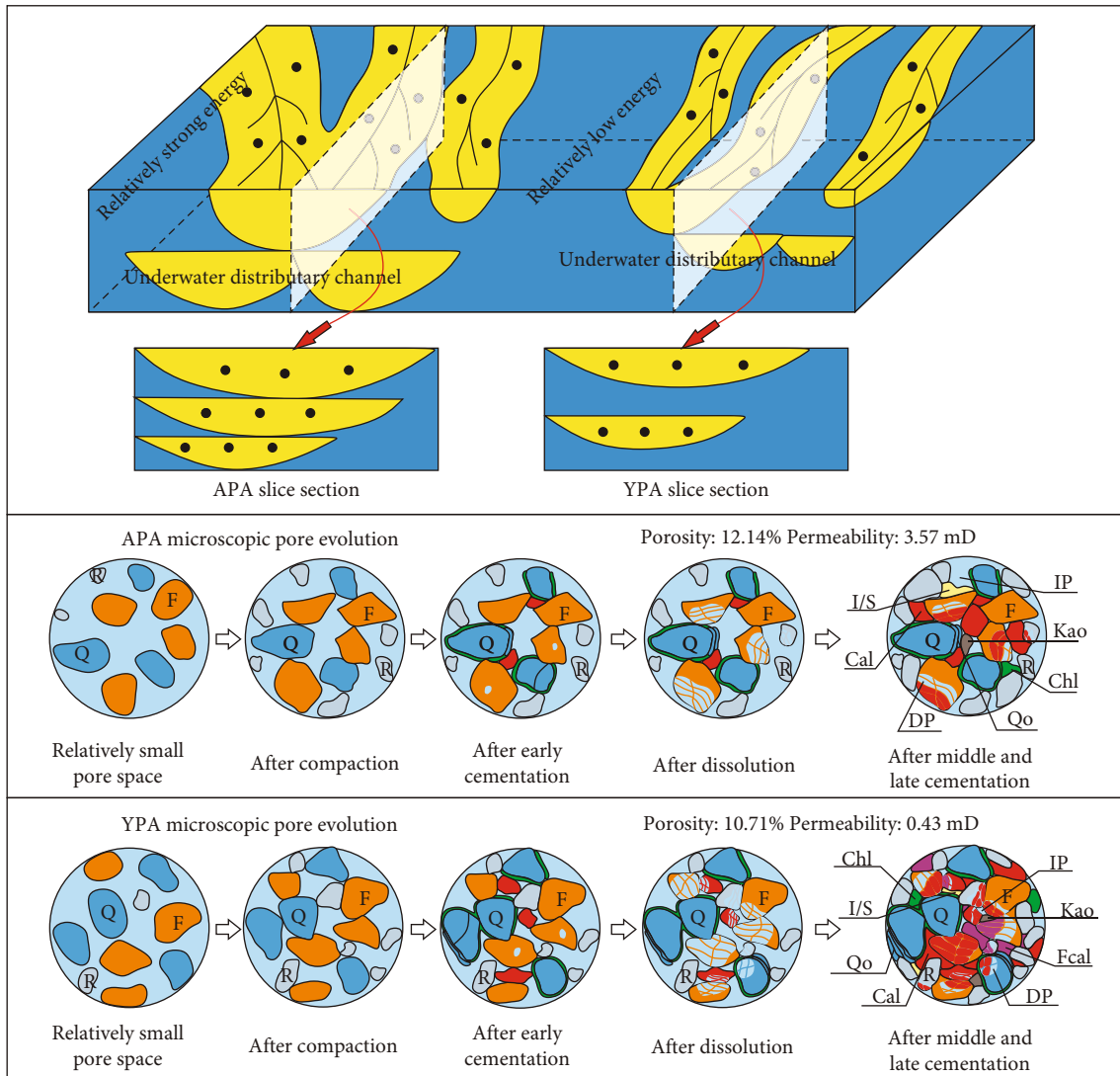
FIGURE 16: Comparison model of the differences in the Chang 8_2 reservoir between the YPA and APA of the Jiyuan area (modified from [9]).

microscope, the intergranular pores of the reservoir in the APA are well preserved due to the formation of the early chlorite film [8]. In addition, the I/S mixed layers are mostly distributed on the grain surface, and the parts filled with pores in the middle and late diagenetic stages are relatively small, so the APA is not greatly affected by the blockage of the pore structure [54]. The YPA reservoir is more thoroughly filled with kaolinite, and the chlorite filling in the YPA reservoir is more thorough than that in the APA reservoir, so the pore reduction in the YPA reservoir is more obvious due to the influence of clay minerals. In terms of the siliceous content, due to the higher degree of diagenetic evolution in the YPA, the secondary growth and development of quartz is relatively greater, so the filling of pores by microcrystalline quartz is also more significant, and the impact on physical properties is also greater than that in the APA.

5.5.3. Differences in Diagenetic Transformation. There is little difference in the types of diagenesis in the APA, but the difference in the diagenetic effect is more significant. Although the APA is slightly larger than the YPA under compaction, the original pore structure is much better than that in the YPA, and many intergranular pores remain [45]. Therefore, after compaction, the grain contact relationship in the APA is looser than that in the YPA. Although the effect of dissolution in the YPA is good, the improvement in porosity is limited [8], the average porosity in the APA cannot be reached after dissolution, and the YPA is much more affected by early and late cementation than the APA. Therefore, cementation and porosity reduction have a great influence on the YPA reservoir, and the cementation of clay minerals is an important factor for the decline in the physical properties of the YPA reservoir. From the perspective of diagenetic facies distribution, the composition of diagenetic facies in the APA is clearly better than that in the YPA, and the development of the most favorable chlorite lining in the residual intergranular pore diagenetic facies is extremely dominant [55]. Moreover, the number of diagenetic facies of

types II, III, and IV in the APA is clearly less than that in the YPA, so the reservoirs in the APA are much better than those in the YPA under the influence of diagenesis.

5.6. Comparison Model of the Genetic Differences. Finally, a comparison model of the differences in the Chang 8_2 reservoir between the APA and YPA of the Jiyuan area is established (Figure 16). The macro distribution of underwater distributary channel sand bodies reveals that in the APA, there is a wider channel, and the larger the sand thickness is, the better the superposition relationship [8] and the stronger the water energy [9]. Compared with the YPA reservoir, more intergranular pores are retained after deposition, which is the basis for the formation of reservoir differences. The evolution of the microscopic pore structure is clearly controlled by diagenesis [8], and the strength and effect of different diagenesis types produce differences in the formation and distribution of mineral particles.

Consistent with the quantitative characterization results of pore evolution, the difference in the pore space after compaction is not large, but after early cementation, the pore space in the APA reservoir is clearly greater than that in the YPA reservoir. Fortunately, the dissolution intensity of the YPA reservoir is higher, resulting in more dissolution pores, which significantly improves the pore space of the reservoir [56]. However, after middle and late cementation and until the end of diagenesis, the YPA reservoir was significantly filled with cementation and clay minerals [14], which greatly reduced the pore space of the reservoir and even the dissolution pores in the previous stage [57], resulting in the final formation of reservoir differences.

6. Conclusion

(1) The reservoir space in the APA is better than that in the YPA, in which the content of intergranular pores is much higher than that in the YPA, but the content of dissolution intergranular pores is much lower than that in the YPA

(2) The physical properties of reservoirs in the APA are far better than those in the YPA. The illite and illite mixed layers in the APA have relatively little effect on the pore throat structure, while the pores in the YPA are filled with kaolinite and chlorite, which is the reason for the deterioration of physical properties

(3) There are differences in the effects of different diagenetic processes on the reservoir. The APA is more compacted than the YPA, but a large number of primary residual intergranular pores are still preserved under the protection of chlorite film. Metasomatism and cementation also have a more significant impact on the YPA reservoir, resulting in the extreme decline in physical properties in the YPA

(4) The diagenetic evolution stage of the APA reservoir is dominated by middle diagenetic stage A, while the diagenetic evolution stage of the YPA reservoir has reached middle diagenetic stage B. The plane distribution of diagenetic facies reflects the difference in the development of reservoirs in the YPA and APA. The diagenetic facies composition of the reservoirs in the APA is better than that in the YPA

(5) Sedimentation is the basis for the development of higher-quality reservoirs in the APA, and the difference in the mineral content further exacerbates the difference in the development of reservoir physical properties. After different types of diagenetic transformation, the APA retains a better pore structure than the YPA

Data Availability

The authors declare that all data in the submitted manuscript are freely available to any researcher wishing to use them for noncommercial purposes, without breaching participant confidentiality. Please contact the corresponding author directly if someone requests the data from this study.

Conflicts of Interest

The authors declare that they have no known competing financial interests or personal relationships that could have appeared to influence the work reported in this paper.

Authors' Contributions

Qiang Tong was assigned in conceptualization, methodology, software, writing-original draft, formal analysis, writing-review and editing, and founding acquisition. Zhaohui Xia was assigned in draft preparation and visualization. Jixin Huang was assigned in validation. Junchang Wu was assigned in project administration. Yusheng Wang was assigned in resources and investigation. Zheng Meng was assigned in supervision. Chaoqian Zhang was assigned in data curation.

Acknowledgments

References

[1] C. N. Zou, Z. Yang, D. Z. Dong et al., "Unconventional source rock formation, distribution and prospect of oil and gas formation," *Earth Science*, vol. 47, no. 5, pp. 1517–1533, 2022.

[2] J. Lai, G. W. Wang, D. C. Wu et al., "Diagenetic facies distribution in high resolution sequence stratigraphic framework of

Chang 8 oil layers in the Jiyuan area," *Geology in China*, vol. 41, no. 5, pp. 1487–1502, 2014.

[3] S. T. Li, Q. Wang, J. A. Zhong et al., "The genesis of sandbody in the shallow delta from Chang 8₁ of Jiyuan area in Ordos Basin," *Natural Gas Geoscience*, vol. 24, no. 6, pp. 1102–1108, 2013.

[4] H. B. Zhao, H. Tang, G. Cheng, D. F. Wang, Y. Q. Zhang, and X. D. Zhang, "Short-term base level cycle and reservoir genesis analysis of Chang 8 oil reservoir set in Jiyuan Oilfield," *Lithologic Reservoir*, vol. 26, no. 2, pp. 89–95+101, 2014.

[5] G. Z. Liu, W. Gao, D. D. Zhang, L. Chen, and A. R. Li, "Sandbody structure and its genesis of shallow-water delta of Chang 8₁ reservoir in Jiyuan area, Ordos Basin," *Lithologic Reservoir*, vol. 31, no. 2, pp. 16–23, 2019.

[6] S. H. Du, F. Xu, A. Taskyn, B. Zhou, G. Kou, and Y. M. Shi, "Anisotropy characteristics of element composition in Upper Triassic "Chang 8" shale in Jiyuan district of Ordos Basin, China: microscopic evidence for the existence of predominant fracture zone," *Fuel*, vol. 253, pp. 685–690, 2019.

[7] Z. B. Chen, Y. S. Zhu, X. J. Chen et al., "Sedimentation and diagenesis of Chang8₂ reservoir in the Yanchang Formation in Jiyuan region, Ordos Basin," *Oil and Gas Geology*, vol. 34, no. 5, pp. 685–693, 2013.

[8] T. T. Yao, Z. D. Bao, Y. L. Zhang et al., "Diagenesis and causes of tight sandstone of Chang 8 reservoirs in the west of Jiyuan Oilfield of Ordos Basin," *Journal of Mineral Petrol*, vol. 36, no. 2, pp. 99–111, 2016.

[9] Y. Wang, L. F. Liu, S. T. Li et al., "Diagenesis and densification process of the Chang 8 interval of Triassic Yanchang Formation, western Jiyuan area, Ordos Basin," *Journal of Palaeogeography*, vol. 19, no. 5, pp. 892–906, 2017.

[10] Y. Kang, G. Chen, W. G. Zhang, J. P. Huang, X. Y. Xia, and J. W. Huo, "Diagenetic densification of Chang 8 sandstone reservoirs and its relationship with hydrocarbon accumulation in Tiebiancheng area, Jiyuan Oilfied, Ordos Basin," *Bulletin of Geological Science and Technology*, vol. 40, no. 2, pp. 64–75, 2021.

[11] J. Lai, G. W. Wang, Y. Chai et al., "Mechanism analysis and quantitative assessment of pore structure for tight sandstone reservoirs: an example from Chang8 oil layer in the Jiyuan area of Ordos Basin," *Acta Geologica Sinica*, vol. 88, no. 11, pp. 2119–2130, 2014.

[12] J. Lai, G. W. Wang, M. Chen et al., "Pore structures evaluation of low permeability clastic reservoirs based on petrophysical facies: a case study on Chang 8 reservoir in the Jiyuan region, Ordos Basin," *Petroleum exploration and development*, vol. 40, no. 5, pp. 606–614, 2013.

[13] S. T. Li, Y. T. Yao, H. W. Qiao et al., "The dissolution characteristics of the Chang 8 tight reservoir and its quantitative influence on porosity in the Jiyuan area, Ordos Basin, China," *Natural Gas Geoscience*, vol. 3, no. 2, pp. 95–108, 2018.

[14] X. Huang, T. T. Li, X. Z. Wang et al., "Distribution characteristics and its influence factors of movable fluid in tight sandstone reservoir: a case study from Chang 8 oil layer of Yanchang formation in Jiyuan Oilfield, Ordos Basin," *Acta Petrolei Sinica*, vol. 40, no. 5, pp. 557–567, 2019.

[15] X. Huang, H. Gao, and L. B. Dou, "Micro pore structure and water-flooding characteristics on tight sandstone reservoir," *Journal of China University of Petroleum (Edition of Natural Science)*, vol. 44, no. 1, pp. 80–88, 2020.

[16] Y. Wang, L. F. Liu, S. T. Li et al., "The forming mechanism and process of tight oil sand reservoirs: a case study of Chang 8 oil layers of the Upper Triassic Yanchang Formation in the western Jiyuan area of the Ordos Basin, China," *Journal of Petroleum Science and Engineering*, vol. 158, pp. 29–46, 2017.

[17] D. Z. Ren, D. S. Zhou, D. K. Liu, F. J. Dong, S. W. Ma, and H. Huang, "Formation mechanism of the Upper Triassic Yanchang Formation tight sandstone reservoir in Ordos Basin–Take Chang 6 reservoir in Jiyuan oil field as an example," *Journal of Petroleum Science and Engineering*, vol. 178, pp. 497–505, 2019.

[18] W. G. Zhang, G. Chen, W. Guo et al., "Comprehensive research of oil-source rock correlation of lower Yanchang formation in Jiyuan Field, Ordos Basin," *Worthwestern Geology*, vol. 53, no. 4, pp. 140–152, 2020.

[19] Y. F. Gu, D. Y. Zhang, and Z. D. Bao, "A new data-driven predictor, PSO-XGBoost, used for permeability of tight sandstone reservoirs: a case study of member of Chang 4+5, western Jiyuan oilfield, Ordos Basin," *Journal of Petroleum Science and Engineering*, vol. 199, article 108350, 2021.

[20] Z. M. Wu, X. Q. Ke, P. Zhang, F. Wen, Q. Tong, and L. Liu, "Sand body architecture of Chang 9 Member in Jiyuan Area, Ordos Basin," *Xinjiang Petroleum Geology*, vol. 43, no. 3, pp. 294–309, 2022.

[21] W. Changyong, Z. Rongcai, and W. Chengyu, "Hydrocarbon accumulation law of lithologic reservoirs of middle Yanchang Formation in Jiyuan area, Ordos Basin," *Lithologic Reservoirs*, vol. 22, no. 2, pp. 84–89+94, 2010.

[22] W. T. Wang, R. C. Zheng, C. Y. Wang, H. H. Wang, Y. L. Han, and C. Y. Wang, "Provenance analysis of the 8th oil-bearing member of Yanchang Formation, Upper Triassic, Jiyuan area, Ordos Basin," *Lithologic Reservoirs*, vol. 21, no. 4, pp. 41–46, 2009.

[23] X. Q. Zhao, Y. L. Wan, C. Yi, S. M. Zhang, and Y. He, "Study on sedimentary facies of Chang 8 member in Jiyuan Oilfield, Ordos Basin," *Lithologic Reservoirs*, vol. 23, no. 4, pp. 94–99, 2011.

[24] X. Yin, S. H. Luo, X. Li, X. F. Men, and W. Xu, "Provenance analysis of Chang 8 period in Jiyuan area of Ordos Basin," *Lithologic Reservoirs*, vol. 20, no. 3, pp. 59–63, 2008.

[25] B. H. Shi, R. K. Li, W. Tian, X. H. Jing, and Z. H. Cai, "Differences of characteristics and genetic of reservoirs in Chang 91 of Yanchang Formation in Jiyuan area, Ordos Basin," *Journal of China University of Petroleum*, vol. 43, no. 4, pp. 1–10, 2019.

[26] B. H. Shi, X. Y. Qin, C. L. Zhang et al., "Insights on factors causing differential enrichment of Chang 6 Member in Jiyuan area, Ordos Basin," *Oil and Gas geology*, vol. 42, no. 5, pp. 1112–1123, 2021.

[27] J. L. Chen, P. Wang, Y. Y. Gao et al., "Application of multiple stepwise regression method in the analysis of the relationship between porosity and tight sandstone: case study of Chang 8 reservoir in Jiyuan area, Ordos Basin," *Natural Gas Geoscience*, vol. 32, no. 9, pp. 1372–1383, 2021.

[28] L. Zhaoyu, L. Wenhou, W. Yue et al., "Characteristics and controlling factors of Chang 8 reservoir of the Jiyuan Area in the Ordos Basin," *Journal of Northwest University*, vol. 50, no. 2, pp. 193–203, 2020.

[29] T. F. Wang, Z. K. Jin, M. J. Chu et al., "Sedimentary environment of the Chang 6 oil-bearing interval of Upper Triassic Yanchang Formation in Jiyuan area, Ordos Basin: Evidences

from geochemical data," *Journal of palaeogeography (Chinese Edition)*, vol. 21, no. 3, pp. 505–516, 2019.

[30] Y. Si, W. X. Zhang, A. X. Luo, B. Sun, and Y. Zhu, "Hydrochemical characteristics and relationship between formation water and hydrocarbon reservoirs for Chang 9 in Jiyuan area," *Journal of China University of Petroleum (Edition of Natural Science)*, vol. 43, no. 2, pp. 25–36, 2019.

[31] H. Yang, J. H. Fu, X. S. Wei, and X. S. Liu, "Sulige field in the Ordos Basin: geological setting, field discovery and tight gas reservoirs," *Marine and Petroleum Geology*, vol. 25, no. 4-5, pp. 387–400, 2008.

[32] C. Y. Wang, C. Y. Wang, X. W. Liang, S. X. Li, H. G. Xin, and R. C. Zheng, "Diagenetic facies of the Chang 8 oil-bearing layer of the Upper Triassic Yanchang formation in the Jiyuan area, Ordos Basin," *Acta Petrolei Sinica*, vol. 32, no. 4, pp. 596–604, 2008.

[33] H. L. Liu, Z. Qiu, L. M. Xu et al., "Distribution of shallow water delta sand bodies and the genesis of thick layer sand bodies of the Triassic Yanchang Formation, Longdong Area, Ordos Basin," *Petroleum Exploration and Development*, vol. 48, no. 1, pp. 123–135, 2021.

[34] Y. B. Bai, J. L. Luo, S. F. Wang et al., "The distribution of Chang 8 tight sandstone oil reservoir of Yanchang formation in Wubao area, central-south of Ordos Basin," *Geology in China*, vol. 40, no. 4, pp. 1159–1168, 2013.

[35] P. Liao, J. Tang, G. Y. Pang, L. Tang, X. F. Ma, and Q. Wang, "Reservoir characteristics and control factors of Chang 8_1 of Yanchang formation of Triassic in Jiyuan region of Ordos Basin," *Journal of Mineral Petrol*, vol. 32, no. 2, pp. 97–104, 2012.

[36] J. A. Udden, "Mechanical composition of clastic sediments," *Geological Society of America Bulletin*, vol. 25, no. 1, pp. 655–744, 1914.

[37] C. K. A. Wentworth, "A scale of grade and class terms for clastic sediments," *Journal of Geology*, vol. 30, no. 5, pp. 377–392, 1922.

[38] D. M. Moore and R. C. Reynolds, *X-ray Diffraction and the Identification and Analysis of clay minerals*, Oxford University Press, Oxford, 1997.

[39] S. Hillier, "Quantitative analysis of clay and other minerals in sandstones by X-ray powder diffraction (XRPD)," in *Clay Mineral Cements in Sandstones*, R. Worden and S. Morad, Eds., pp. 213–251, International Association of Sedimentologist, Special Publication, Oxford, International, 1999.

[40] Y. J. Shi, L. Xiao, Z. Q. Mao, and H. P. Guo, "An identification method for diagenetic facies with well logs and its geological significance in low-permeability sandstones: a case study on Chang 8 reservoirs in the Jiyuan region, Ordos Basin," *Acta Petrolei Sinica*, vol. 32, no. 5, pp. 820–828, 2011.

[41] J. Lai, G. W. Wang, L. X. Huang et al., "Quantitative classification and logging identification method for diagenetic facies of tight sandstones," *Bulletin of Mineralogy, Petrology and Geochemistry*, vol. 34, no. 1, pp. 128–138, 2015.

[42] B. Liu, H. L. Wang, X. F. Fu et al., "Lithofacies and depositional setting of a highly prospective lacustrine shale oil succession from the Upper Cretaceous Qingshankou Formation in the Gulong sag, northern Songliao Basin, Northeast China," *AAPG Bulletin.*, vol. 103, no. 2, pp. 405–432, 2019.

[43] B. Liu, X. Q. Zhao, X. F. Fu et al., "Petrophysical characteristics and log identification of lacustrine shale lithofacies: a case study of the first member of Qingshankou Formation in the Songliao Basin, Northeast China," *Interpretation*, vol. 8, no. 3, pp. SL45–SL57, 2020.

[44] SY/T 5368, "Petroleum and Gas Industry Standard," in *People's Republic of China*, State Bureau of Petroleum and Chemical Industry (in Chinese), 2000.

[45] S. T. Li, J. L. Yao, W. W. Mou et al., "The dissolution characteristics of the Chang 8 tight reservoir and its quantitative influence on porosity in the Jiyuan area, Ordos Basin, China," *Journal of Natural Gas Geoscience*, vol. 3, no. 2, pp. 95–108, 2018.

[46] Y. Li, S. Li, W. Mou, and C. C. Yan, "Influences of clay minerals on physical properties of Chang 6 tight sandstone reservoir in Jiyuan area, Ordos Basin," *Natural Gas Geoscience.*, vol. 28, no. 7, pp. 1043–1053, 2017.

[47] SY/T 6285, "Petroleum and Gas Industry Standard," in *People's Republic of China*, National Energy Administeation (in Chinese), 2011.

[48] Y. Q. Qu, W. Sun, R. D. Tao, B. Luo, L. Chen, and D. Ren, "Pore-throat structure and fractal characteristics of tight sandstones in Yanchang Formation, Ordos Basin," *Marine and Petroleum Geology.*, vol. 120, article 104573, 2020.

[49] Z. Li, S. H. Wu, D. L. Xia, S. He, and X. Zhang, "An investigation into pore structure and petrophysical property in tight sandstones: a case of the Yanchang Formation in the southern Ordos Basin, China," *Marine and Petroleum Geology*, vol. 97, pp. 390–406, 2018.

[50] M. Wang, Z. Yang, C. Shui, Z. Yu, Z. Wang, and Y. Cheng, "Diagenesis and its influence on reservoir quality and oil-water relative permeability: a case study in the Yanchang formation Chang 8 tight sandstone oil reservoir, Ordos Basin, China," *Open Geosciences*, vol. 11, no. 1, pp. 37–47, 2019.

[51] Y. F. Cui, G. W. Wang, S. J. Jones et al., "Prediction of diagenetic facies using well logs - a case study from the upper Triassic Yanchang Formation, Ordos Basin, China," *Marine and Petroleum Geology*, vol. 81, pp. 50–65, 2017.

[52] J. W. Cui, S. Li, and Z. G. Mao, "Oil-bearing heterogeneity and threshold of tight sandstone reservoirs: a case study on Triassic Chang7 member, Ordos Basin," *Marine and Petroleum Geology*, vol. 104, pp. 180–189, 2019.

[53] J. F. Chen, J. L. Yao, Z. G. Mao et al., "Sedimentary and diagenetic controls on reservoir quality of low-porosity and low-permeability sandstone reservoirs in Chang10_1, Upper Triassic Yanchang Formation in the Shanbei area, Ordos Basin, China," *Marine and Petroleum Geology*, vol. 105, pp. 204–221, 2019.

[54] SY/T 5477, "Petroleum and Gas Industry Standard," in *People's Republic of China*, State of Economic and Trade commission (in Chinese), 2003.

[55] K. L. Xi, Y. C. Cao, K. Y. Liu et al., "Diagenesis of tight sandstone reservoirs in the Upper Triassic Yanchang Formation, southwestern Ordos Basin, China," *Marine and Petroleum Geology*, vol. 99, pp. 548–562, 2019.

[56] S. L. St and W. Mou, "Diversity of the Triassic Chang 8_1 low permeability reservoirs in Jiyuan and Xifeng area, Ordos Basin," *Acta Sedimentologica Sinica*, vol. 36, no. 1, pp. 166–175, 2018.

[57] Z. Wang, X. Luo, Y. Lei et al., "Impact of detrital composition and diagenesis on the heterogeneity and quality of low-permeability to tight sandstone reservoirs: an example of the Upper Triassic Yanchang Formation in Southeastern Ordos Basin," *Journal of Petroleum Science and Engineering*, vol. 195, article 107596, 2020.